7. SITE 1043[1]

Shipboard Scientific Party[2]

HOLE 1043A

Position: 9°39.273′N, 86°11.160′W

Start hole: 0400 hr, 8 December 1996

End hole: 0545 hr, 11 December 1996

Time on hole: 73.75 hr (3.07 days)

Seafloor (drill-pipe measurement from rig floor, mbrf): 4324.0

Water depth (drill-pipe measurement from sea level, m): 4312.7

Distance between rig floor and sea level (m): 11.3

Total depth (drill-pipe measurement from rig floor, mbrf): 4606.3

Penetration (mbsf): 282.3

Coring totals:

Type: APC; No: 3; Cored: 26.4 m; Recovered: 26.75 m (101.3%)
Type: XCB; No: 27; Cored: 255.9 m; Recovered: 197.85 m (77.3%)
Total: RCB; No: 30; Cored: 282.3 m; Recovered: 224.60 m (79.6%)

Formation:

Unit T1 (0–150.57 mbsf): Clay, silty clay and breccia (?Pliocene–Pleistocene)
Subunit U1B (150.57–195.95 mbsf): Diatomaceous ooze and clay with diatoms (early–late Pleistocene)
Subunit U2A (193.95–245.63 mbsf): Silty clay and clay (late Pliocene–early Pleistocene)
Subunit U2B (245.63–263.71 mbsf): Calcareous clay, clay with nannofossils, and silty clay (late Miocene?–early Pliocene)
Subunit U3A (263.71–282.30 mbsf): Siliceous nannofossil ooze and calcareous clay with nannofossils (late Miocene)

HOLE 1043B

Position: 9°39.259′N, 86°11.143′W

Start hole: 0545 hr, 11 December 1996

End hole: 0345 hr, 13 December 1996

Time on hole: 46.0 hr (1.92 days)

Seafloor (drill-pipe measurement from rig floor, mbrf): 4321.0

Water depth (drill-pipe measurement from sea level, m): 4309.6

Distance between rig floor and sea level (m): 11.4

Total depth (drill-pipe measurement from rig floor, mbrf): 4803.3

Penetration (mbsf): 482.3

Logging while drilling

Principal results: Lithologic objectives included description of the complete section through the wedge, décollement, and underthrust units, and determination of whether material was missing at the top of the underthrust section. One lithologic unit was defined above the underthrust section at Site 1043, Unit T1 (Fig. 1). Below the décollement, Subunits U1B through U3A of the Cocos Plate reference section were recognized. Unit T1 (?Pliocene–Pleistocene; 0–150.57 mbsf) consists mainly of thick intervals of clay and silty clay interbedded with relatively thin intervals of matrix-supported breccia. The breccias consist of firm lumps of claystone, siltstone, and ooze embedded in a clayey to sandy matrix. Thin layers and small pods of volcanic ash, and minor interbeds of silt and sand, appear throughout Unit T1. Minor clasts of Pliocene and Miocene limestone and calcareous ooze suggest that older calcareous units have contributed debris to the unit. Subunit U1B, Unit U2, and Subunit U3A at Site 1043 are similar to the units defined at the reference site, Site 1039; Subunit U1A was not recovered. Three structural domains were defined at Site 1043. Domain I (0–141.3) is the mildly deformed part of the wedge toe, and coincides with all but the lowermost part of Unit T1. Domain II (141.3–150.57 mbsf) is the more intensely deformed décollement zone at the base of Unit T1, and Domain III represents the underthrust section of Units U1B–U3A, which are only slightly deformed.

Within the Site 1043 wedge sediments, reversals in age-depth distribution can be used to define the locations of thrust faults. A foraminifer marker with an age of 1.77 Ma, the Chron C2n onset at 125 mbsf, and the occurrence of a diatom marker with an age less than 0.62 Ma below that interval, indicates that an age inversion occurs between 125 and 130 mbsf, arguing strongly for the existence of a thrust fault. Another possible thrust fault is indicated by an age-depth inversion defined by nannofossil and foraminifer datums and the Brunhes/Matayama (B/M) magnetic polarity boundary, which matches an interval of low bulk density and high porosity at 25–30 mbsf in the logging-while-drilling (LWD) logs of Hole 1043B. Below the décollement, age-depth relationships can be calculated using a combination of biostratigraphic and paleomagnetic information. In Unit U1 (150–194 mbsf), age-depth rates range from 52 to 40 m/m.y., within Unit U2 (194–263 mbsf) the rate is 15 m/m.y., and within Unit U3 (263 mbsf–total depth [TD]) the rate is less than 12 m/m.y. Comparing the depth of the B/M boundary at this site (180 mbsf, 30 m below the décollement) with the depth of this polarity transition at Site 1039 (59 mbsf), indicates that the portion of lithostratigraphic Unit U1 above the B/M boundary has been thinned by ~30 m by some combination of faulting and compaction at this site.

Geochemistry objectives included determining the pathways and potential sources of pore fluids through the deformed wedge, décollement, and underthrust sections. Two regions show narrow zones of very low density on the LWD logs. One is 74–77 mbsf and the other is in the décollement zone (148–157 mbsf). Each of these depths is associated with major anomalies in Cl, Si, K, PO_4, and salinity. These anomalies are zones of relative freshening of the pore waters. The source of the fresher water could be from dehydration of clay minerals or input from meteoric water. Effects of gas hydrates could influence some of the anomalies, but cannot explain the entire effect. Post-cruise analyses will be required to distinguish these alternatives. Sulfate decreases rapidly with depth in the upper 15–20 mbsf, beneath which it is completely reduced through the décollement. Immediately beneath the décollement, sulfate jumps to relatively high levels and continues to approach that of seawater with depth in the hole. Alkalinity behaves opposite to that of sulfate, increasing rapidly in the top 15 mbsf, staying high until the décollement, dropping to lower values below the décollement, and then gradually decreasing with depth in the underthrust section. Alkalinity approaches seawater values at 270 mbsf.

[1]Kimura, G., Silver, E.A., Blum, P., et al., 1997. *Proc. ODP, Init. Repts.*, 170: College Station, TX (Ocean Drilling Program).
[2]Shipboard Scientific Party is given in the list preceding the Table of Contents.

Previous Chapter Table of Contents Next Chapter

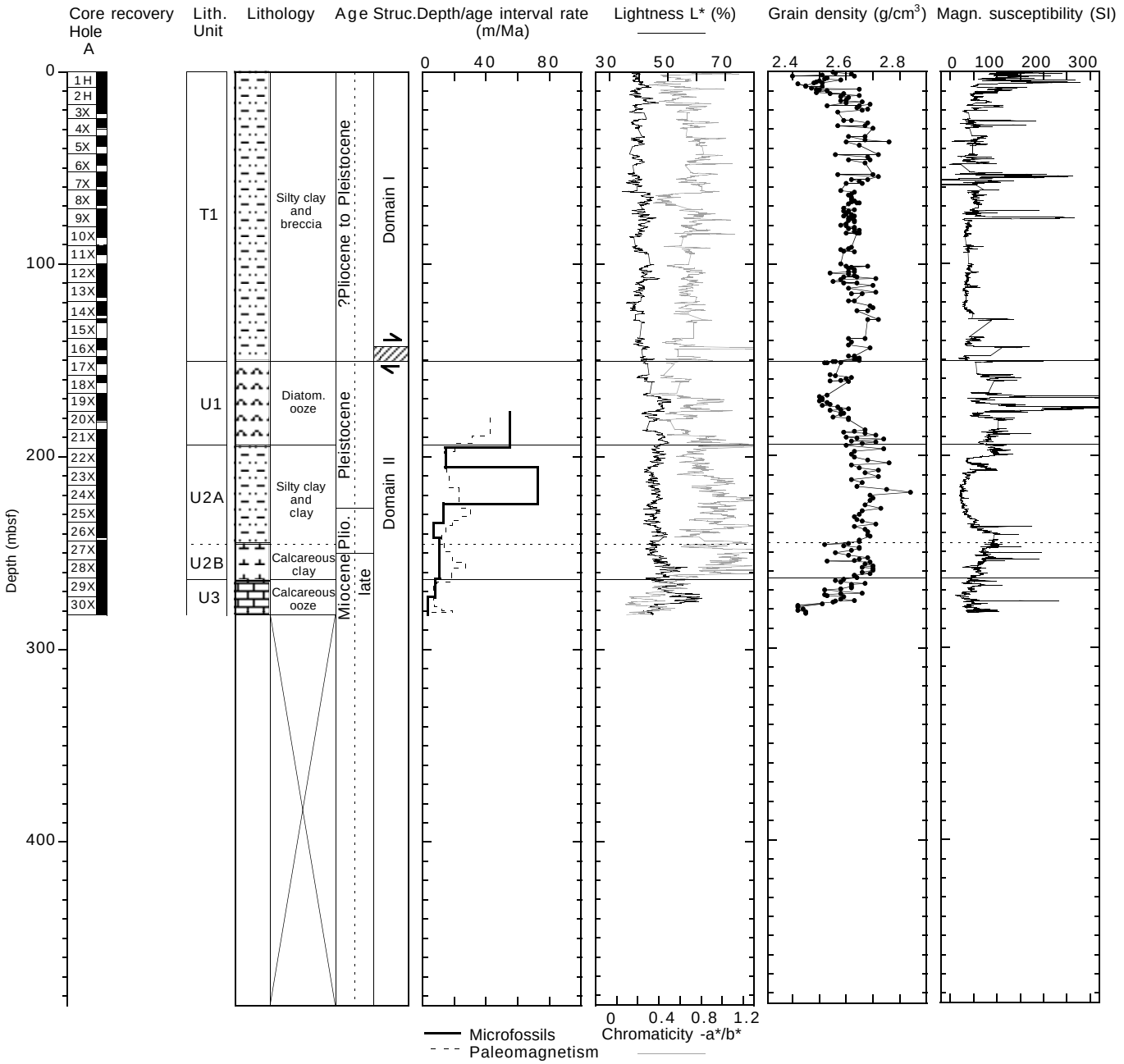

Figure 1. Graphical representation and summary plots of shipboard core and downhole measurements. Explanation of data types and their acquisition are found in the "Explanatory Notes" chapter (this volume). Shipboard descriptions of data are found in relevant sections in this chapter. LWD = logging while drilling; SGR = spectral gamma ray (total counts); and CGR = computed gamma ray (total counts minus contribution of uranium). Hatching in the structure column indicates Domain II.

Physical properties measurements, including downhole observations, were central to the objectives of Site 1043. Significant changes in thickness and reduction in density were noted between correlative units at Sites 1039 and 1040. Site 1043 is located at a position intermediate in terms of potential dewatering. Bulk density and porosity in the wedge section show a complex pattern, including a number of intervals where the consolidation state decreases somewhat with depth (Fig. 1). Some of these may be related to increased fracturing, which affects the downhole logs more than core measurements. The most prominent negative excursion of bulk density down to 1.1 g/cm^3 from the baseline (1.8 g/cm^3) occurs in the interval 72–75 mbsf, which is correlated to the interval characterized by a geochemical anomaly. A broad negative excursion down to 1.3 g/cm^3 occurs in the interval 88–107 mbsf. All negative excursions in the upper 150 mbsf are correlated with the relatively large standoff of up to 7.5 cm, as indicated by the differential caliper log. At the décollement zone itself, physical properties exhibit a steep gradient, possibly indicating some shear-enhanced compaction in addition to dewatering of the underthrust section produced by the weight of the overlying wedge section. The trends through the underthrust section match those in the reference section (Site 1039), but density, *P*-wave velocity, and resistivity are higher, whereas porosity is somewhat lower. A distinct increase in density occurs at 285 mbsf, which coincides with the top of nannofossil ooze in Hole 1039B. It is apparent that only the upper part of the underthrust section (150–190 mbsf) has dewatered significantly, and in the interval below this (190–250 mbsf) the physical properties suggest a modest reversal in the consolidation state.

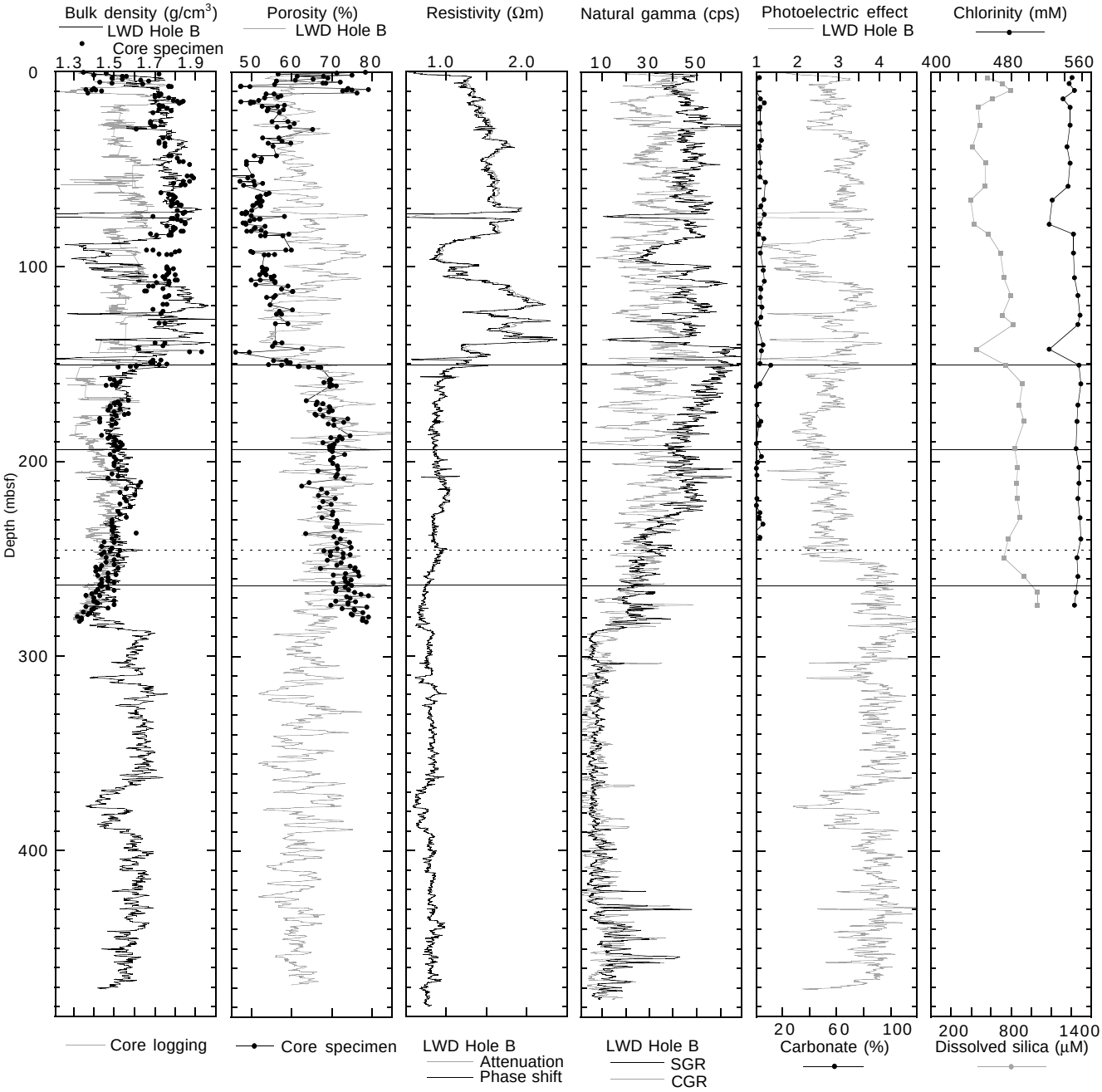

Figure 1 (continued).

In summary, drilling at Site 1043 attained all of our objectives. We cored and logged complete sections through the décollement, acquiring excellent quality materials. Geochemistry provided clean, detailed signals of the fluid behavior with depth, as it has all through the leg, and the fluid pathways required by the geochemistry coincide with zones of very low density, seen in the logs and the structural geology of the cores.

BACKGROUND AND SCIENTIFIC OBJECTIVES

Site 1043 is located 400 m northeast from the toe of the continental slope, 1 km from Site 1040. The purpose of drilling at Site 1043 was to obtain a complete section through the décollement to supplement that from Site 1040 and to obtain a complete set of LWD logs through the décollement and much of the underthrust section. The primary scientific objectives at this site are similar to those of Site 1040, with the following elaboration. The rate of change of thickness of the underthrust hemipelagic sequence (Units U1 and U2) is highest at the location of Site 1043. This rate of change may correspond with a high rate of dewatering of the underthrust section as well.

Site 1040 showed that the underthrust section was reduced in thickness relative to the reference site (Site 1039) to ~67% in the hemipelagic section and 80% in the pelagic chalk. The details of these differences remain to be determined by post-cruise research. In addition, the hemipelagic section showed evidence of anomalous dips at Site 1040, suggesting deformation of this section beneath the décollement. A problem occurred while drilling Site 1040; the RCB core barrel caused a number of spiral twists of the cores above the décollement, essentially destroying much of the primary structural fabric. The décollement is much shallower at Site 1043 (~150 mbsf) than

at Site 1040 (371 mbsf), providing a better opportunity of getting through it with fewer drilling difficulties and without the use of the RCB.

Site 1040 showed much less offscraping than expected based on interpretation of seismic-reflection data. About 10% offscraping was expected from the seismic, but only about 1% was observed. Site 1043 was designed to test whether or not offscraping is temporally and spatially intermittent and whether deformation of the underthrust hemipelagic sediments develop soon after subduction. The seismic stratigraphy of Site 1043 (Fig. 2, "Site 1040" chapter, this volume) is similar beneath the décollement to that of Site 1039, although both the hemipelagic and pelagic sections are decreased in thickness. The décollement reflection at Site 1043 is negatively polarized, as it is in Site 1040. It is difficult to discern primary geologic structure based on the reflective character above the décollement. This site is separated from Site 1040 by a normal fault that displaces the underthrust strata and the basement reflection. Site 1040 lies on the downthrown side of this fault. No significant faults separate the Cocos Plate stratigraphy at Sites 1039 and 1043.

OPERATIONS

Hole 1043A

Hole 1043A was spudded with the bit at 4322.5 m below rig floor (mbrf). Core 170-1043A-1H recovered 8.01 m of sediment (Tables 1, 2). Advanced hydraulic piston corer (APC) Core 2H failed to bleed off pressure, indicating incomplete stroke in the firm seafloor material. Extended core barrel (XCB) coring began with Core 3X and continued through Core 18X at a depth of 167.1 mbsf. A small amount of fill and slightly elevated pump pressure was identified at 157.5 mbsf, after Core 17X; however a single 30-bbl sweep of sepiolite drilling mud cleaned up the hole, and no further problems were encountered. A rapid increase in rate of penetration (ROP) occurred while cutting Core 18X, which only took 5 min to cut. Although the formation softened, the material remained quite stiff. The APC barrel was deployed for Core 19H (167.1–176.6 mbsf) in an attempt to get an undisturbed core sample. The barrel did achieve full stroke, and recovered 9.83 m of high quality core. Coring resumed with the XCB system, because the sediment was even more highly compacted than on the previous core, and it was deemed unwise to be advancing the hole beneath the décollement with the core liner in the pipe. Coring continued with the XCB to a total depth of 282.3 mbsf. Coring was abandoned at this point to allow time for two final LWD holes at Sites 1043 and 1042, respectively. The hole was displaced with 75 bbl of 10.5 lb/gal mud. As the pipe was tripped, the vessel was offset 50 m to the southeast for spudding Hole 1043B.

A single temperature measurement with the Davis-Villinger Temperature Probe (DVTP) was attempted after Core 170-1043A-4X at 33.4 mbsf. However, the data were bad because the formation was too hard. Subsequent temperature measurements were canceled.

Evidence of hydrate nodules was seen beginning with Core 6X. Hydrocarbon levels were highly variable and dropped significantly below the top of the underthrust zone identified in Core 17X at ~150 mbsf. Methane values, as measured by headspace gas analysis, ranged from 81 to 237,615 ppmv above the décollement and from 165 to 6 ppmv below the décollement. Ethane values ranged from 48 to 2 ppmv above the décollement, with nothing below Core 18X (167.1 mbsf). Propane measured 0–6 ppmv, and no higher hydrocarbons were identified.

Hole 1043B

Hole 1043B was to be the first of two back-to-back LWD holes. The jars were pressure tested (low 500 and high 3000 psi) before making up the LWD bottom-hole assembly (BHA) with a tricone drill bit. The compensated dual resistivity (CDR) and compensated

Table 1. Coring summary for Site 1043.

Core	Date (Dec. 1996)	Time (UTC)	Depth (mbsf)	Length cored (m)	Length recovered (m)	Recovery (%)
170-1043A-						
1H	08	2210	0.0-8.0	8.0	8.01	100.0
2H	08	2305	8.0-16.9	8.9	8.91	100.0
3X	09	0105	16.9-24.4	7.5	4.64	61.8
4X	09	0405	24.4-33.4	9.0	5.40	60.0
5X	09	0610	33.4-42.8	9.4	5.56	59.1
6X	09	0835	42.8-52.2	9.4	5.87	62.4
7X	09	1055	52.2-61.6	9.4	7.52	80.0
8X	09	1255	61.6-71.2	9.6	7.90	82.3
9X	09	1455	71.2-80.7	9.5	9.51	100.0
10X	09	1655	80.7-90.3	9.6	5.50	57.3
11X	09	1840	90.3-99.9	9.6	4.54	47.3
12X	09	2015	99.9-109.5	9.6	9.83	102.0
13X	09	2155	109.5-119.2	9.7	7.66	78.9
14X	09	2330	119.2-128.7	9.5	7.17	75.5
15X	10	0105	128.7-138.3	9.6	1.64	17.1
16X	10	0240	138.3-147.9	9.6	6.25	65.1
17X	10	0420	147.9-157.5	9.6	3.94	41.0
18X	10	0540	157.5-167.1	9.6	4.05	42.2
19H	10	0650	167.1-176.6	9.5	9.83	103.0
20X	10	0855	176.6-186.0	9.4	5.32	56.6
21X	10	1040	186.0-195.6	9.6	9.16	95.4
22X	10	1215	195.6-205.2	9.6	9.87	103.0
23X	10	1405	205.2-214.8	9.6	9.29	96.8
24X	10	1550	214.8-224.5	9.7	9.75	100.0
25X	10	1730	224.5-234.1	9.6	9.85	102.0
26X	10	1900	234.1-243.7	9.6	7.83	81.5
27X	10	2015	243.7-253.3	9.6	9.87	103.0
28X	10	2155	253.3-263.0	9.7	9.85	101.0
29X	10	2320	263.0-272.6	9.6	9.86	103.0
30X	11	0110	272.6-282.3	9.7	9.69	99.9
Coring totals:				282.3	224.07	79.4

Note: UTC = Universal Time Coordinated.

Table 2. Coring section summary for Site 1043.

Leg	Site	Hole	Core	Type	Top (mbsf)	Bottom (mbsf)	Advancement	Section number	Liner length (m)	Curated length (m)	Map interval top (mbsf)	Map interval bottom (mbsf)	Map type
170	1043	A	1	H	0	8	8	1	1.5	1.5	0	1.5	STD
170	1043	A	1	H	0	8	8	2	1.5	1.5	1.5	3	STD
170	1043	A	1	H	0	8	8	3	1.5	1.5	3	4.5	STD
170	1043	A	1	H	0	8	8	4	1.5	1.5	4.5	6	STD
170	1043	A	1	H	0	8	8	5	1.5	1.5	6	7.5	STD
170	1043	A	1	H	0	8	8	6	0.23	0.23	7.5	7.73	STD
170	1043	A	1	H	0	8	8	7	0.28	0.28	7.73	8.01	STD
170	1043	A	2	H	8	16.9	8.9	1	1.5	1.5	8	9.5	STD
170	1043	A	2	H	8	16.9	8.9	2	1.5	1.5	9.5	11	STD
170	1043	A	2	H	8	16.9	8.9	3	1.5	1.5	11	12.5	STD

Note: STD = standard.

This is a sample of the table that appears on the volume CD-ROM.

density neutron (CDN) LWD tools were made up as part of a standard BHA, including the McCullough mechanical drilling jars. The drill string was tripped to the seafloor, filling the pipe every 40 stands. Hole 1043B was spudded and drilling continued at a target rate of penetration (ROP) of 25 m/hr, to a depth of 196 mbsf where the rate was increased to 35 m/hr. Drilling continued without incident to a total depth of 4803.3 m (482.3 mbsf), when a drastic reduction in ROP and increased torque indicated that the target reflector had been reached. Basement for the site had been projected at ~490.0±10 mbsf. It was assumed that the hole was stopped on basement, or indurated sediments directly overlying the basement.

No problems were experienced penetrating the décollement, and only a single 30-bbl sepiolite mud sweep was required during the drilling. The pill was circulated at a depth of 453.4 mbsf, when a slight increase in pump pressure was recognized by the driller. The hole was displaced with 140 bbl of 10.5 lb/gal mud before being abandoned. The vessel was then offset back to Site 1042.

LITHOSTRATIGRAPHY AND STRUCTURES

Drilling at Site 1043 penetrated through the toe of the sedimentary wedge into the underthrust sequence. One new lithologic unit (Unit T1) is defined at Site 1043 (Table 3; Fig. 1). Below the décollement, Subunits U1B through U3A of the Cocos Plate reference section (see "Site 1039" chapter, this volume) were recognized.

Unit T1 (Pliocene?–Pleistocene; 0–150.57 mbsf) consists mainly of thick intervals of clay and silty clay interbedded with relatively thin intervals of matrix-supported breccia. Thin layers and small pods of volcanic ash, and interbeds of silt and sand, appear throughout Unit T1. Minor clasts of Pliocene and Miocene limestone and calcareous ooze suggest that older calcareous units have contributed debris to the unit.

Because Subunit U1B, Unit U2, and Subunit U3A at Site 1043 are so similar to the units defined at the reference site, only the major characteristics are included here. The reader is referred to the "Site 1039" chapter (this volume) for details.

Three structural domains were defined at Site 1043. Domain I (0–141.3 mbsf) is the little-deformed part of the wedge toe, coinciding with all but the lowermost part of Unit T1. Domain II (141.3–150.57 mbsf) is the more intensely deformed décollement zone at the base of Unit T1, and Domain III represents the mildly deformed underthrust section of Subunits U1B–U3A.

Description of Units

Unit T1: Clay, Silty Clay, and Breccia

Interval: 170-1043A-1H-1, 0 cm, to 17X-2, 117 cm
Thickness: 150.57 m
Depth: 0–150.57 mbsf
Age: Pliocene?–Pleistocene

Unit T1 occupies the toe of the sedimentary wedge. The sediments are firm to very firm from near the base of Core 170-1043A-1H downward, but remain unlithified. The unit consists of clay and silty clay alternating with thin intervals of sedimentary breccia (Tables 3, 4). The breccia intervals appear to represent a fining-downward sequence, becoming progressively finer grained and thinner downward through the unit. Breccias make up ~15% of the total stratigraphic thickness of Unit T1. Widely scattered clasts of claystone occur throughout the clayey intervals, even where no breccia layers appear to be present.

Clay and Silty Clay

The dominant lithology in Unit T1 is clay and silty clay (Fig. 2), and even the breccias consist mainly of clay(stone) and silt(stone) fragments. Most of the unit consists of monotonous intervals of medium to dark olive-green clay and silty clay. Variations in color to a lighter olive green reflect 5- to 10-cm-thick layers of slightly more biogenic material (Fig. 2). Some layers suggested by color contrasts are up to 1–2 m thick. The sediment is poorly sorted; even the clays have trace to common amounts of silt and fine sand scattered throughout (Table 5). Dark gray interbeds of clayey silt, sandy silt, and silty sand range from a few centimeters thick to 0.5 m thick, but are most commonly 2–10 cm thick. A dark gray, fine- to coarse-sand bed in interval 170-1043A-16X-4, 33–112 cm, contains glauconite, feldspar, quartz, amphibole, pumice, glass, red chert(?), and other lithic fragments.

Fossils visible in the cores include sand-sized benthic foraminifers, shell fragments, wood and plant debris, small sponges, and a shark tooth. Bioturbation, evident from numerous burrows filled with lighter green to yellowish brown clay, probably has mixed the fine-grained sediment and destroyed most of any original layering that may have been present. Burrow fills tend to be richer in diatoms and nannofossils than the surrounding clay. Small pods of volcanic ash, sand, and silt 1–2 cm thick are also common and probably represent burrow fillings.

Smear-slide observations (Table 5) reveal that Unit T1 is characterized by abundant clay and ubiquitous silt- to sand-sized grains of volcanic glass. Other silt- to sand-sized grains include quartz, feldspar, rock fragments (typically pumice and polycrystalline quartz), glauconite, and crystalline phosphate in trace to common amounts. Rare grains of green and brown amphibole, pyroxene, and biotite are also seen. Biogenic components in the clay and silty clay include trace to common amounts of foraminifers, diatoms, and fish remains, as well as trace amounts of nannofossils, radiolarians, sponge spicules, pollen, and spores.

Table 3. Site 1043 lithostratigraphic units.

Unit	Subunit (Unit T1 lithologies in parentheses)	Intervals	Thickness (m)	Depth (mbsf)	Age
T1: clay, silty clay, and breccia (0-150.57 mbsf)	(Matrix-supported breccia, clay, and silty clay)	1H-1, 0 cm, to 3X-1, 38 cm	17.28	0-17.28	Pleistocene
	(Silty clay and clay with volcanic ash)	3X-1, 38 cm, to 11X-2, 0 cm	74.52	17.28-91.80	early Pleistocene
	(Matrix-supported breccia and clay)	11X-2, 0 cm, to 12X-1, 18 cm	8.28	91.80-100.08	
	(Silty clay and clayey silt with ash)	12X-1, 18 cm, to 15X-1, 70 cm	29.32	100.08-129.40	
	(Breccia and clay)	15X-1, 70 cm, to 15X-CC, 48 cm	0.94	129.40-130.34	
	(Silty clay with sandy silt, clay)	15X-CC, 48 cm, to 17X-2, 117 cm	20.23	130.34-150.57	early Pliocene
U1: diatomaceous ooze (150.57-193.95 mbsf)	U1B: diatomaceous ooze and clay with diatoms	17X-2, 117 cm, to 21X-6, 45 cm	43.38	150.57-193.95	early to late Pleistocene
U2: silty clay and calcareous clay (193.95-263.71 mbsf)	U2A: silty clay and clay	21X-6, 45 cm, to 27X-2, 43 cm	51.68	193.95-245.63	late Pliocene to early Pleistocene
	U2B: calcareous clay, clay with nannofossils, and silty clay	27X-2, 43 cm, to 29X-1, 71 cm	18.08	245.63-263.71	late Miocene? to early Pliocene
U3: calcareous ooze (263.71-282.30 mbsf)	U3A: siliceous nannofossil ooze and calcareous clay with nannofossils	29X-1, 71 cm, to 30X-CC, 20 cm	>18.59	263.71-282.30	late Miocene

Table 4. Site 1043 lithologic summary.

Core	Major lithology	Color	Fossils	Diagenesis	Minor lithology	A/C/T
170-1043A-						
1H	1) Matrix-supported breccia in silty clay with diatoms	Olive green	C: forams, diatoms	T: framboids	1) Olive green sandy silt w/forams	T
	2) Clay with diatoms		T-A: nannofossils		2) Clasts of claystone, ashy claystone, chalk, diatom clayst. in breccia	C
			T: rads, spicules, fish parts, pollen, wood, shark tooth		3) Medium gray ashy clay pod	T
2H	1) Matrix-supported breccia	Olive green	C: diatoms	T-C-: framboids	Clasts of claystone, nanno. chalk, diatom clayst., ashy claystone, silty claystone, clayey silt in breccia	C
	2) Clast supported breccia		T-C: rads, spicules			
	3) Diatomaceous clay		T: nannos, forams, silicos, fish parts, peloids, plants			C
3X	1) Matrix-supported breccia	Olive green	T: diatoms, rads	T: framboids	Clasts of dark olive green silty claystone with trace of nannos, forams	C
	2) Silty clay					

Notes: Ash below Core 18X was thixotropic at time of recovery. A = abundant, C+ = very common, C = common, C- = somewhat common, T = trace. Rads = radiolarians, forams = foraminifers, nannos = nannofossils, spicules = sponge spicules, framboids = pyrite framboids, and fish = fish bones/parts.

This is a sample of the table that appears on the volume CD-ROM.

Dark gray to black spots within the olive-green clay are enriched in pyrite framboids and small pyrite concretions. Some pyrite concretions are tubular, suggesting they may have filled burrows. Disseminated pyrite framboids are nearly ubiquitous in smear slides (Table 5). Some diatoms and/or spores are filled with framboids, and some glauconite grains contain pyrite framboids as well. A siderite vein was observed in interval 170-1043A-13X-2, 70–78 cm.

Breccia

The uppermost part of Unit T1 (Tables 3, 4) consists of ~17 m of brownish gray to grayish green matrix-supported breccias interbedded with dark olive-green to brownish to greenish clay, silt, and minor sand. Breccias also dominate two thinner intervals, at 91.8–100.08 mbsf (8 m thick) and 129.4–130.34 mbsf (0.9 m thick; Table 3).

The poorly sorted breccia beds range in thickness from 8 to 100 cm. The largest clasts are cobble sized, ranging from 3 to 5 cm (Fig. 3), but most are granule to pebble sized. Clasts are typically angular to subangular, but some breccia layers include subrounded clasts (Fig. 4). Most breccia layers are graded (fining upward) but a few are reverse-graded (coarsening upward). Typically the basal contacts of these breccias are ill defined rather than sharp and scoured (Fig. 4). Most clasts consist of firm sediment or lithified material. Clast compositions identified in smear slides (Table 5) include olive-green diatomaceous claystone, dark brown claystone, dark green silty claystone, and green ashy claystone. Matrix of the breccia layers consists either of very poorly sorted sand-silt-clay mixtures (Fig. 3) or silty clay (Fig. 4). Breccia matrix components are dominantly terrigenous, indistinguishable from the silty clay, silt, and sand that make up most of Unit T1.

Finer grained interbeds within the breccias (Fig. 5) consist mainly of olive-green to green clay and silty clay, with minor pods and thin layers of volcanic ash or ash mixed with clay. The breccia-dominated intervals grade into the clay-dominated intervals described above.

Carbonate Clasts and Layers

Isolated clasts, concretions, and thin layers of limestone, chalk, and calcareous ooze are scattered throughout the breccias as well as the finer grained intervals (Fig. 5). In the uppermost breccia interval, calcareous clasts include light gray siliceous clayey nannofossil ooze and white nannofossil ooze with diatoms. Nannofossils in the latter clast are Pleistocene. A light brown, thinly laminated chalk clast at 92.05 mbsf contains late Miocene nannofossils. Yellowish brown or yellowish green calcareous ooze and chalk also occur as thin layers and discontinuous stringers a few centimeters thick (Fig. 6). Near the base of Unit T1 such interbeds are stretched and pulled apart.

Volcanic Ash

In addition to the silt- and sand-sized grains of volcanic glass and pumice disseminated throughout Unit T1, layers of light to dark gray volcanic ash are sparsely interbedded with the clay and breccia intervals. Ash is also preserved as burrow fill and small drilling-disturbed pods. Some ash layers contain clay, suggesting reworking by bioturbation, and some are clearly graded with sharp scoured bases; these typically contain other terrigenous components such as glauconite grains, as well as biogenic components such as nannofossils and diatoms. Some ash layers exhibit internal laminations and possible cross bedding (Fig. 7); others are massive and appear to be homogeneous. Ashes observed in Unit T1 range from light gray vitric ashes to green lithic-vitric and crystal-lithic-vitric ashes. One bright emerald green ash layer consists of crystal-lithic (pumice) ash mixed with clay. Vitric ashes are composed mainly of clear glass with rare brown glass. Crystal-rich ashes contain euhedral to subhedral plagioclase, amphibole, and rare biotite or pyroxene, as well as subhedral quartz grains. Quartz and plagioclase are generally present in subequal amounts (Table 5).

Unit U1: Diatomaceous Ooze

Interval: 170-1043A-17X-2, 117 cm, to 21X-6, 45 cm
Thickness: 43.38 m
Depth: 150.57–193.95 mbsf
Age: early–late Pleistocene

Subunit U1A: Not Recovered at Site 1043

Subunit U1B: Diatomaceous Ooze, Clay with Diatoms

Interval: 170-1043A-17X-2, 117 cm, to 21X-6, 45 cm
Thickness: 43.38 m
Depth: 150.57–193.95 mbsf
Age: early–late Pleistocene

The 5.55-m-thick turbidite-rich Subunit U1A of Site 1039 (see “Site 1039” chapter, this volume) was not observed at Site 1043. Immediately below the structurally defined base of the décollement zone in Core 170-1043A-17X, diatoms begin to increase, going from trace amounts at the top of Core 170-1043A-17X to common below the base of the décollement zone, to abundant near the top of Core 170-1043A-18X (Table 5).

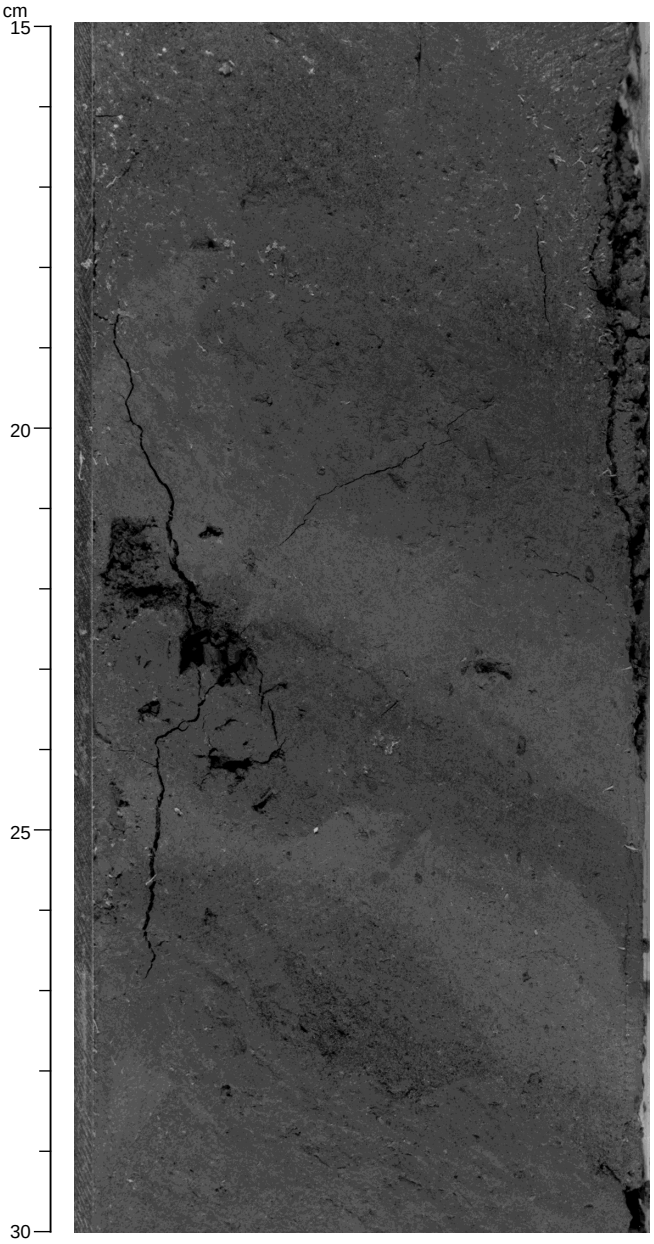

Figure 2. Olive-green clay that makes up most of Unit T1, interbedded with dark green to gray silty clay and sandy silt and light green calcareous clay (interval 170-1043A-8X-4, 15–30 cm).

Smear-slide data across the boundary zone indicate gradually increasing diatom abundances relative to silt and clay. From a sedimentological standpoint, from 149.36 to 157.55 mbsf, a distance of about 8 m, the base of the décollement zone is not as sharply defined as at Site 1040.

From Section 170-1043A-18X-1 to its base in Section 170-1043A-21X-6 (Table 3), Subunit U1B consists of olive-green to grayish green diatomaceous ooze with disseminated volcanic glass, but few other terrigenous components (Tables 4, 5). Quartz and feldspar are present in trace amounts. Nannofossils, present only in trace amounts above the décollement, become common in Core 18X and fluctuate from common to trace amounts well into Subunit U2A.

At Site 1043, Subunit U1B is very similar to the corresponding unit observed at Site 1039. It is generally homogeneous, with common to abundant pyrite concretions up to 3 cm long and 2 mm across. Pyrite is also concentrated in pods, layers, and burrows. *Zoophycos* is the most common recognizable burrow. The subunit includes interbeds of light to dark gray vitric and crystal-vitric ash (Fig. 8), as well as ash-rich silt and sand (Table 4), that are similar to those seen at Site 1039. Many of the ash layers and most of the silt and sand layers are graded with scoured bases and laminated tops (Fig. 8), suggesting that they were deposited by turbidity currents.

Unit U2: Silty Clay, Clay, and Calcareous Clay

Interval: 170-1043A-21X-6, 45 cm, to 29X-1, 71 cm
Thickness: 69.76 m
Depth: 193.95–263.71 mbsf
Age: late Miocene?–early Pleistocene

Subunit U2A: Silty Clay and Clay

Interval: 170-1043A-21X-6, 45 cm, to 27X-2, 43 cm
Thickness: 51.68 m
Depth: 193.95–245.63 mbsf
Age: late Pliocene–early Pleistocene

Subunit U2B: Calcareous Clay, Clay with Nannofossils, Silty Clay

Interval: 170-1043A-27X-2, 43 cm, to 29X-1, 71 cm
Thickness: 18.08 m
Depth: 245.63–263.71 mbsf
Age: late Miocene?–early Pliocene

At Site 1039, Unit U2 was defined by a sharp decrease in biogenic components accompanied by a corresponding increase in terrigenous material, particularly clay (see “Site 1039” chapter, this volume). A similar change defines the top of Unit U2 at Site 1043. Within less than 5 m, from 190 to 195 mbsf, diatoms drop from abundant to trace, and all terrigenous components increase to common or abundant (Table 5). Unit U2 is extensively bioturbated (Fig. 9).

Subunit U2A at Site 1043 consists of olive-green to grayish green clay and silty clay with minor interbeds of vitric and crystal-vitric volcanic ash (Table 4). Although diatoms and nannofossils are present, they are not abundant, and the subunit is dominated by clay plus silt- to sand-sized grains of quartz, feldspar, and disseminated volcanic ash (Table 5).

At Site 1043, Subunit U2B is defined by the appearance of calcareous interbeds in Core 170-1043A-27X. Subunit U2B consists of olive-green silty clay interbedded with lighter green siliceous nannofossil ooze and calcareous clay with nannofossils. Some intervals of Liesegang banding occur (Fig. 10), generally localized around concretions or, in some cases, around ash layers.

Unit U3: Siliceous Nannofossil Ooze and Calcareous Clay with Nannofossils

Interval: 170-1043A-29X-1, 71 cm, to 30X-CC, 20 cm
Thickness: >18.59 m
Depth: 263.71–282.30 mbsf
Age: late Miocene

Subunit U3A: Siliceous Nannofossil Ooze and Calcareous Clay with Nannofossils

Interval: 170-1043A-29X-1, 71 cm, to 30X-CC, 20 cm
Thickness: >18.59 m
Depth: 263.71–282.30 mbsf
Age: late Miocene

The biogenic components increase downhole through Subunit U2B and biogenic-rich layers increase in number and thickness until the sediment is dominated by biogenic components rather than terrigenous components. The top of Subunit U3A at Site 1043 is defined at the striking color change from green calcareous clay to ivory white

Table 5. Site 1043 smear-slide descriptions.

Sample number							Depth	Imp.		Size				Composition													Fossils									Sediment or rock name	Comment
Leg	Site	Hole	Core	Type	Section	Interval (cm)	mbsf	Major lithology	Minor lithology	Med.-coarse sand	Fine sand	Silt size	Clay size	Quartz	Feldspar	Clay	Rock fragments	Volcanic glass	Amphibole	Glauconite	Phosphate	Dolomite	Carbonate	Micrite	Opaque	Framboid	Nannofossils	Foraminifers	Diatoms	Radiolarians	Silicoflagellates	Sponge spicules	Fish remains	Peloids/pellets	Other		
170	1043	A	1	H	1	19	0.19	X		T	C-	C+	A	C+	C	A	C	T	C-	C-					T	T		C+	T		T			T	Olive green sandy silty clay with diatoms	Other = wood & plant fragments. Diatoms, spores are filled with framboids
170	1043	A	1	H	2	56	2.06		X		T	C	A		T	A		C+	T						T	T					T				Medium gray pod of ashy clay	
170	1043	A	1	H	2	73	2.23		X	T	C+	A	C+	C-	C	C+	C-	C		C-	T		T		T	T		C	C-			T	T		T	Olive green clayey sandy silt with foraminifers	Other = pollens and spores, some filled with framboids
170	1043	A	1	H	3	121	4.21		X		T	C	A	T	T	A		C+											T				T			Dark green ashy clay	
170	1043	A	1	H	4	96	5.46	X			T	C-	A	T	T	A	T	C-		C-	T							T	C	T						Olive green clay with diatoms	
170	1043	A	1	H	CC	20	7.93		X			T	A		T	T		T						C-	C-		A		C	T		T		T		Clast of light brown laminated nannofossil ooze with diatoms Pleistocene 13.6-15.6 Ma	
170	1043	A	2	H	1	4	8.04		X		T	T	A	T		C+		T						T			A	T	C	C-	T	C-	T			Light gray clast of siliceous clayey nannofossil ooze	
170	1043	A	2	H	1	102	9.02		X			T	A	T	T	A		C+									T		C-			T				Green clast of ashy claystone	
170	1043	A	2	H	1	118	9.18		X		T	C	A	T	C-	A	C-	C	T	T	T				T	C-			T			T				Dark green clast of silty claystone	
170	1043	A	2	H	2	60	10.10	X			T	C	A	T	T	C+	T			T		T				T	T			C+			T	T		Olive green diatomaceous claystone	

Notes: Imp. = important. A = abundant, C+ = very common, C = common, C- = somewhat common, T+ = strong traces, T = trace, and blank box = not observed.

This is a sample of the table that appears on the volume CD-ROM.

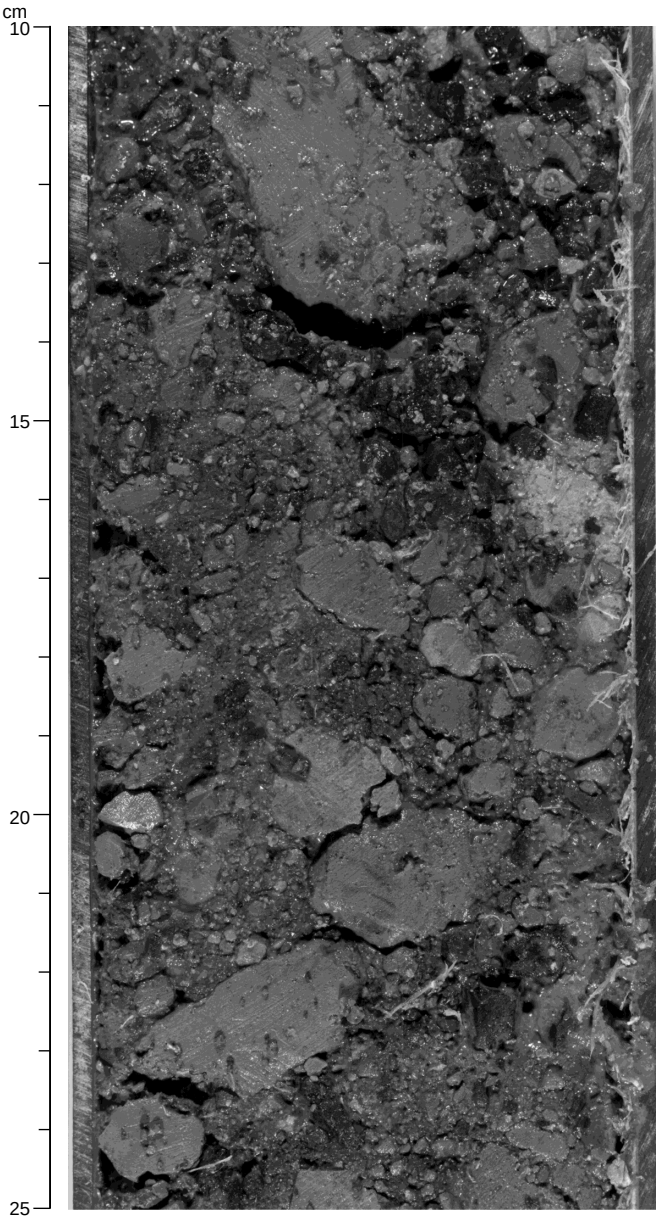

Figure 3. Unit T1 breccia consisting of angular clasts of pebble- to cobble-sized claystone in a matrix of sand- and granule-sized clasts of the same composition (interval 170-1043A-2H-1, 10–25 cm).

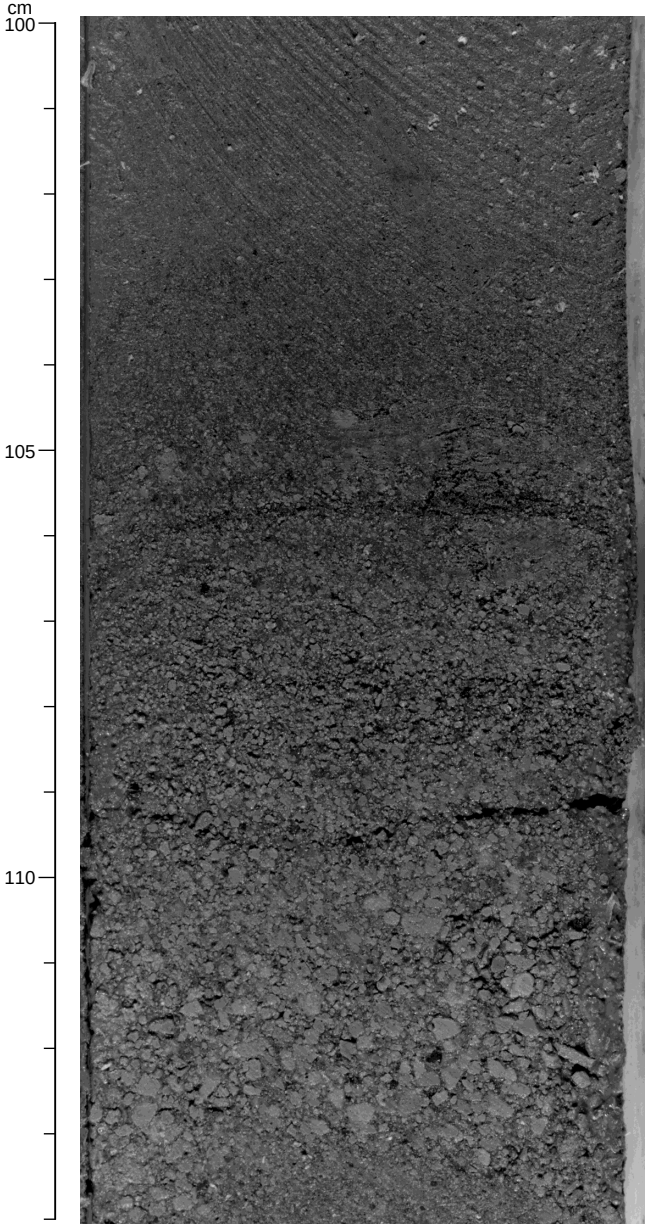

Figure 4. Unit T1 breccia consisting of subangular to subrounded clasts of small pebbles and granules grading upward through a sequence of sand, silt, and clay. The clay overlying this breccia is typical of the majority of Unit T1 (interval 170-1043A-2H-2, 100–114 cm).

nannofossil ooze in Core 170-1043A-29X. The base of Subunit U3A was not reached at Site 1043.

Subunit U3A consists of ivory white siliceous nannofossil ooze interbedded with light green calcareous clay and dark green clay with diatoms. Although nannofossils are the most abundant biogenic component in this unit, diatoms are very common to abundant as well. Few terrigenous components other than volcanic glass are observed (Table 5). The distinctive style of extremely well-developed, mostly *Zoophycos*, burrows in Subunit U3A (Fig. 11) is diagnostic of this unit.

Structural Geology

Structural observations and measurements made at Site 1043 (Table 6; Fig. 12) indicate that the 282 m of sediments recovered can be divided into three distinct structural domains: Domain I, the sedimentary wedge toe; Domain II, the décollement zone; and Domain III, the underthrust section.

Domain I (0–141.3 mbsf) is the structurally heterogeneous toe of the wedge where subduction-related deformation interacts with the extremely dynamic depositional environment. The boundary between Domain I and Domain II is gradational, and we arbitrarily place it at the first occurrence of closely spaced fracture networks that show polished surfaces typical of incipient scaly fabric. Domain II comprises the roughly 10-m thickness of the décollement zone, from 141.3 to 150.57 mbsf, where the deformation fabric is most strongly developed. The base of Domain II appears to be very sharp where the structural signature shows an abrupt change to less deformed sediment. Domain III (150.57–282.30 mbsf) extends from the base of the décollement zone to the bottom of Hole 1043A. Brittle deformation features decrease from 150 to ~190 mbsf. Sediments from 190 to

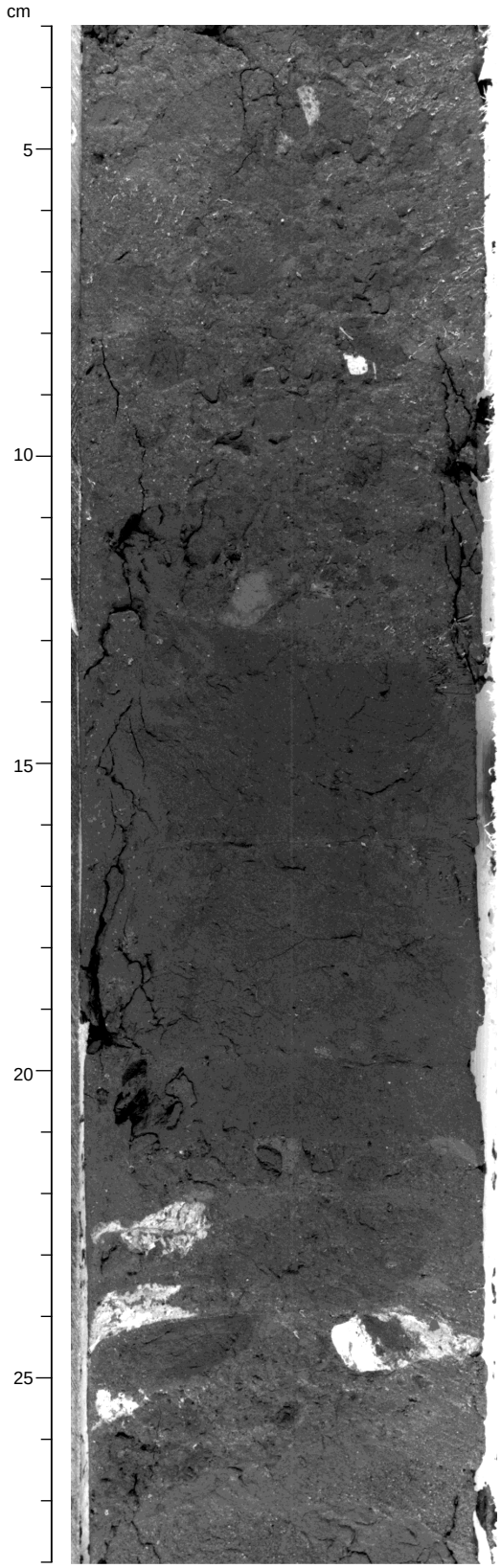

Figure 5. Clasts of light brown to white nannofossil chalk in breccia layers of Unit T1. The clast on the right side of the core at 24 cm contains Miocene nannofossils. The photograph shows parts of two breccias separated by a layer of dark olive-green silty clay. Most clasts in the breccias are claystone (interval 170-1043A-11X-2, 3–28 cm).

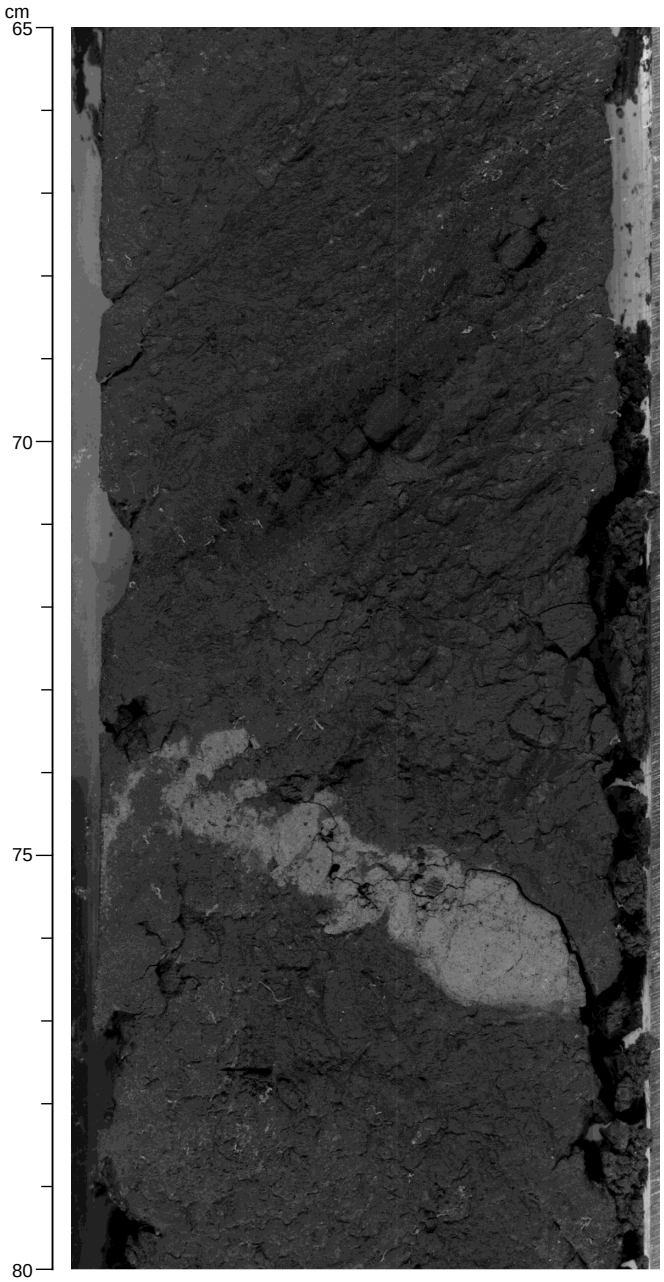

Figure 6. Interbed of light yellowish brown chalk, Unit T1. This layer, located less than a meter above the base of the décollement zone, exhibits boudinage, internal tension fractures, and incipient dismemberment. Because this is in a zone of strong spiral disturbance, deformation is probably at least partly drilling disturbance (interval 170-1043A-17X-2, 65–80 cm).

~255 mbsf are almost undeformed, but deformation increases from ~255 to TD at 282.30 mbsf.

At Site 1043, deformation is indicated by inclined bedding, fissility, core-scale faults with small (millimeter to centimeter) offsets, fracture networks, and incipient scaly fabric. A system of very closely spaced parallel joints, spaced 0.5–1.0 cm apart, that are distributed over the entire rock volume is also observed. The origin of the incipient scaly fabric was much debated, and it proved impossible to determine with certainty whether the features are artificial (drilling induced) or natural. The recovery of an APC core, Core 170-1043A-19H, from just below the décollement domain and above one of these incipient fabric intervals is especially revealing regarding the effects of drilling disturbance. Core 170-1043A-19H has a generally mas-

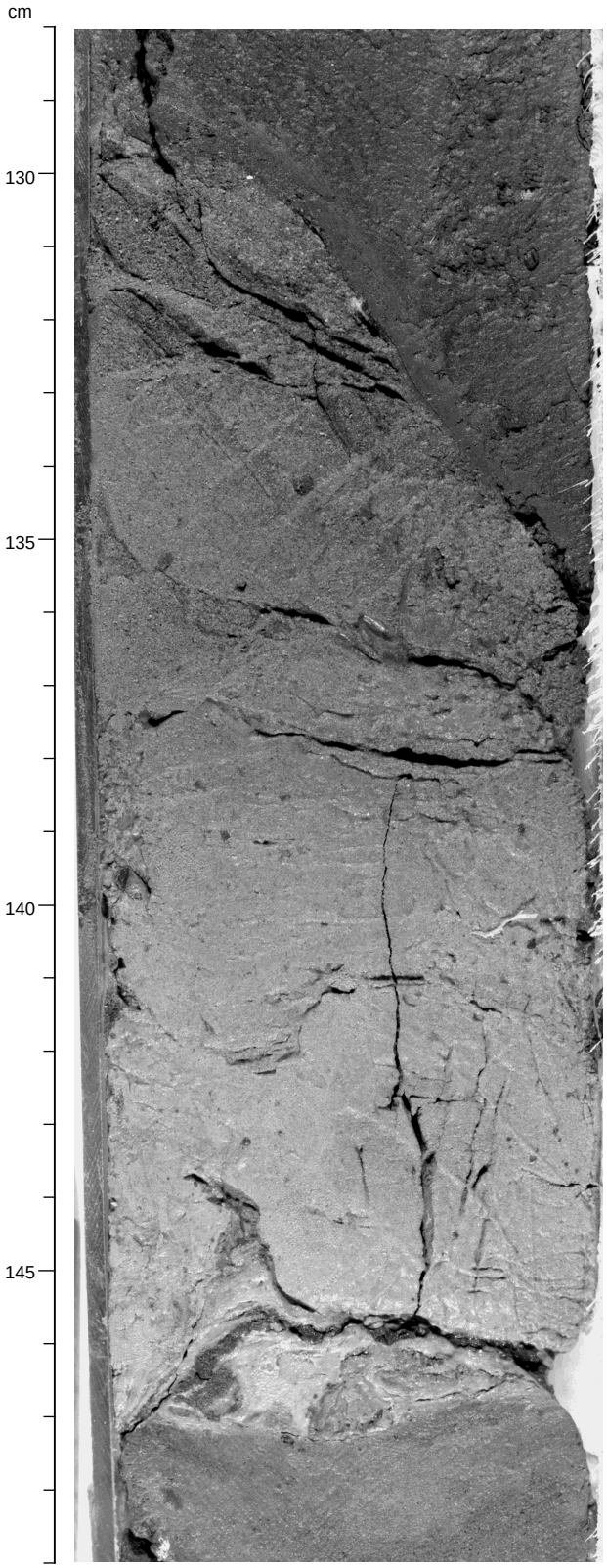

Figure 7. Layer of light green lithic-vitric ash with clay in Unit T1. The upwards gradation into clay-rich ash with thin laminations suggests deposition by subaqueous transport. The originally sharp base has been modified by fluid expulsion from a thinner vitric ash layer below, probably as a result of drilling disturbance. Most of the ashes observed below 140 mbsf at Site 1043 were thixotropic (interval 170-1043A-17X-1, 128–149 cm).

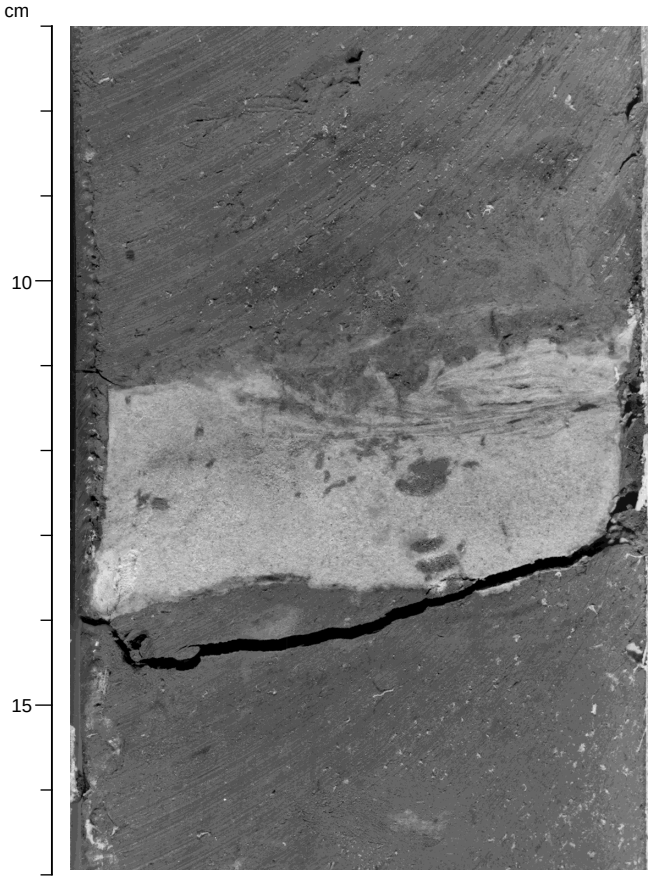

Figure 8. Typical olive-green silty clay of Subunit U1B, with an interbed of light gray vitric ash. The ash has a sharp scoured base and grades upward into a zone of thin cross laminations. Burrows in both ash and clay are typical of this unit (interval 170-1043A-19H-3, 7–17 cm).

sive appearance with only a few microfaults, whereas Core 170-1043A-20X is intersected by closely spaced joints. On the other hand, more fractured intervals do occur within individual cores, as in Core 170-1043A-21X, where just the first 60 cm shows this fabric.

At Site 1043, XCB coring produced an extreme drilling disturbance, similar to that observed in RCB cores at Site 1040, manifested as quasi-continuous torsional plastic deformation of the cores over intervals of some meters (Fig. 12), referred to as “spiral drill disturbance.” Even though this spiral disturbance occurs over a much more restricted interval than at Site 1040, it affects some of the most critical intervals such as the base of the décollement zone.

We were able to reorient a limited number of bedding dips into true geographic coordinates, using natural remanence directions (see “Biostratigraphy and Magnetostratigraphy” section, this chapter) on Core 170-1043-19H, in which APC coring prevented biscuiting (Fig. 13).

Domain I: The Sedimentary Wedge Toe (0–141.50 mbsf)

Domain I corresponds to the main body of Unit T1 with the exception of the décollement zone. Bedding is highly variable in this interval, but does not show any consistent trend (Fig. 12). A few microfaults and fractured intervals are scattered over the entire domain. Cores 170-1043A-8X and 9X exhibit some closely spaced fracture systems. Core 170-1043-9X also contains some thin deformation bands and pinch-and-swell structures. Core 170-1043A-8X is characterized by an intense form of spiral drill disturbance, precluding the use of orientation data. Below Core 170-1043A-9X, the degree of de-

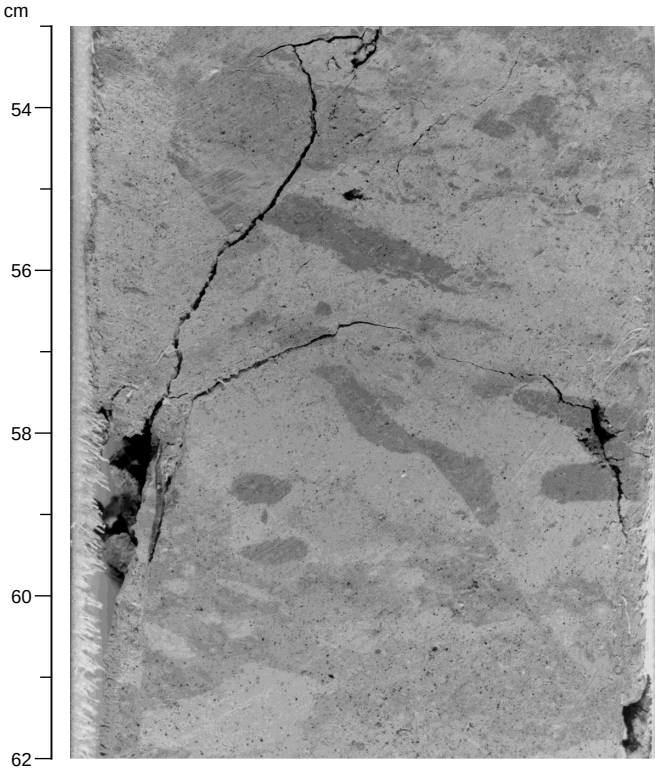

Figure 9. Bioturbated light green silty clay and light gray calcareous clay of Subunit U2B. A normal microfault offsets some of the burrows. *Zoophycos* trace at 62 cm (interval 170-1043A-28X-6, 53–62 cm).

formation decreases until Core 170-1043A-13X, where it begins to gradually increase down to the décollement.

The sediments in Domain I are generally fairly well compacted. Some of the cores display fissility, as in the intervals 16.90–42.80 mbsf, 61.60–99.90 mbsf, and 119.20–141.50 mbsf, whereas others are massive.

No unequivocal evidence for discrete fault zones or strongly localized shearing was observed within Domain I. However, evidence suggests at least one structural discontinuity. Small-scale deformation bands and fracture systems in Cores 170-1043-8X and 9X suggest a deformed zone at about 75 mbsf. A sharp increase in ethane and propane content (Fig. 14), a chlorinity minimum, and an increase in porosity all suggest a fluid conduit, and at this depth LWD results indicate a density and resistivity anomaly (see "Physical Properties" section, this chapter). The most likely explanation for the coincidence of the deformed zone with these other features is a fault.

The base of Domain I (interval 170-1043A-15X through 16X-2, 128.70–141.50 mbsf) exhibits several zones in which the claystone has been fragmented into centimeter- to millimeter-scale fragments. These fragments have rhombic shapes, and some are lenticular with polished surfaces. An age inversion in the interval 125–130 mbsf is defined by foraminifers, diatoms, and magnetostratigraphy (see "Biostratigraphy and Magnetostratigraphy" section, this chapter), suggesting a possible thrust fault. In that interval, small-scale (2 cm) fracture networks are present. However, based on the available structural and lithologic data, a major fault is not obvious.

Domain II: Décollement Zone (141.50–150.57 mbsf)

Beginning at interval 170-1043A-16X-2, 112 cm, and continuing to the bottom of 17X-2, a zone of anastomosing, discontinuous, polished, and finely interpenetrative fracture systems marks the décollement zone (Fig. 15). We place the top of the décollement zone at this

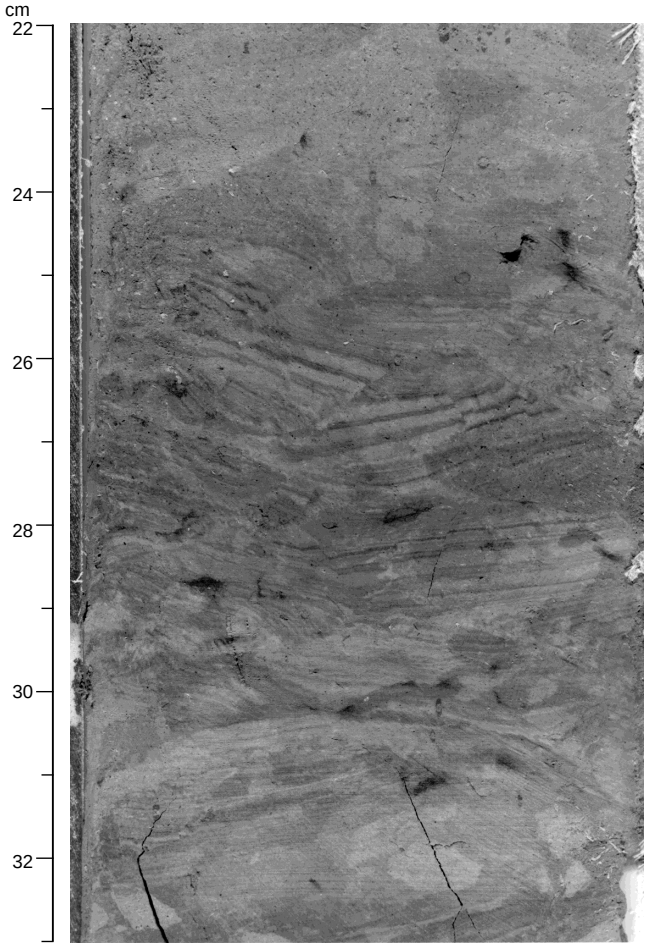

Figure 10. Liesegang rings within calcareous clay and silty clay in an intensely microfaulted zone of Subunit U2B (interval 170-1043A-28X-7, 22–33 cm).

apparent increase in deformation at 141.50 mbsf, although the exact location is uncertain because of poor core recovery and the gradual increase in deformational features. In contrast, the bottom is sharp and well defined. The lower boundary coincides with the contact between Units T1 and U1.

As was observed at Site 1040, the décollement zone does not exhibit true scaly fabric, but rather it exhibits only an incipient scaly fabric with little evidence of shearing. The lowermost part of the décollement zone is characterized by plastically deformed silty clay. Paleomagnetic measurements indicate that the bottom of the décollement at Site 1043 has been affected by extreme spiral drill disturbance, rendering suspect the observed structural features. We did observe a change in lithology to a more clay-rich interval, which may indicate a change in formation rheology.

A minimum in chloride concentration and other pore-water geochemical anomalies occur in Section 170-1043A-16X-3 (see "Geochemistry" section, this chapter), possibly indicating that the observed intense fracture systems form a fluid conduit at the top of the décollement zone.

Domain III: Underthrust Section (150.50–282.30 mbsf)

Beginning in Section 170-1043A-17X-3 and continuing to the total depth of 282.30 mbsf, the structural style changes. This change, although well marked, is not as abrupt as at Site 1040. Core 170-1043A-18X exhibits some fractures with unpolished surfaces, and

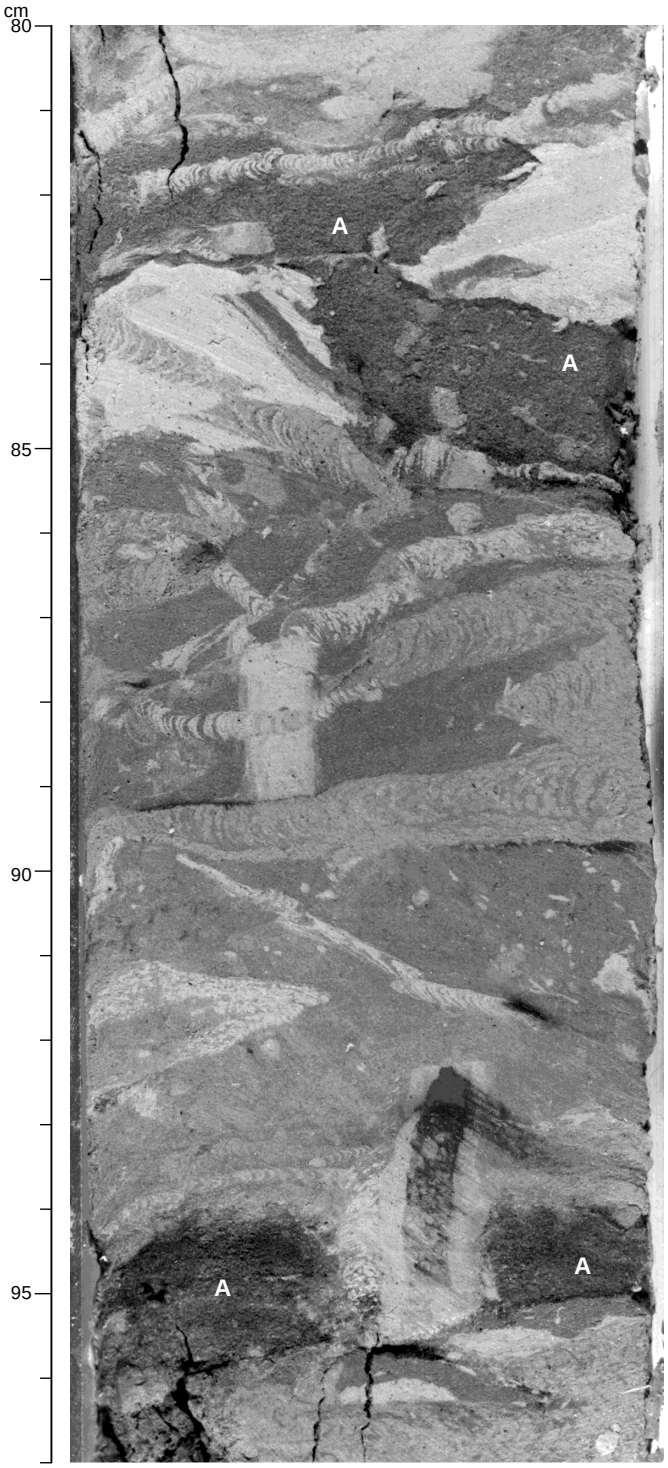

Figure 11. The *Zoophycos*-burrowed zone of Subunit U3A. This distinctive zone where light gray to ivory white calcareous ooze is mixed with darker green and gray siliceous oozes is characteristic of Subunit U3A at all three sites where it was recovered. Two dark gray layers of vitric ash (A) can be seen at 82–86 cm, and 94–96 cm (interval 170-1043A-29X-2, 80–97 cm).

some stretched layers. Discrete normal microfaults occur in the same core. Bedding dips remain scattered down to Core 170-1043A-21X, about 190 mbsf, and only below that depth are they consistently shallow (Fig. 12). These features suggest that some deformation may result from the overriding décollement.

The sediments of Domain III become increasingly compacted toward the base. Cores 170-1043A-20X and 21X exhibit fissility and a perpendicular set of rough fractures. The intersections between these two sets of surfaces break the sediment into elongated fragments. Core 170-1043A-19H lacks any fissility.

Below Core 170-1043A-21X, sediments generally are massive, nearly to the bottom of the hole. Starting at Core 170-1043A-28X (~250 mbsf), a number of microfaults, especially normal ones, exhibit displacements of a few millimeters (Figs. 9, 12). Similar minor extensional features were described both seaward and arcward at Sites 1039 and 1040.

Core 170-1043A-19H, taken with the APC, gave us the opportunity to reorient three bedding dips into true geographic coordinates using natural remanence directions (see "Biostratigraphy and Magnetostratigraphy" section, this chapter; Fig. 13). The orientations form a cluster and exhibit an average 31° dip toward 019°, indicating a landward dip in the uppermost part of the underthrust section.

Discussion

Unit T1 is characteristic of a slope deposit formed by fine-grained submarine grain flows alternating with debris flows. The isolated lithoclasts within the silty clay may have been ferried downslope by fairly dense grain flows or may have slid individually. The poorly sorted debris flows suggest that relatively little fluid was incorporated within the sediment during movement. The well-sorted sedimentary breccias were probably transported by more fluid turbidity currents. A likely source of the coarse, angular breccia clasts is fault scarps higher on the slope of the sedimentary wedge.

Deformation within the décollement zone is much less intense than at Site 1040, presumably because Site 1043 is much closer to the tip of the wedge. Although structural features exhibit a sharp break at the boundary, sediments at the base of the décollement zone do not undergo as sharp a compositional change as at Site 1040, perhaps because of the emplacement of one or more thin thrust packages above the décollement of similar lithology to material just below. Porewater geochemistry, although sampled only at 10-m intervals, also argues for a more diffuse flow regime (see "Geochemistry" section, this chapter).

Discontinuities in fossil ages (see "Biostratigraphy and Magnetostratigraphy" section, this chapter) were observed at 21.5 mbsf, near the base of the first breccia interval in Unit T1; at 130 mbsf, within a monotonous clay interval in Unit T1; and at 235 mbsf, within Subunit U2A. These discontinuities may be explained in three ways: as erosional unconformities, as faults, or as hiatuses in deposition. Results from geochemistry, physical properties, and LWD support their interpretation as faults. The paleomagnetic record also indicates that an age inversion occurs across the décollement zone.

BIOSTRATIGRAPHY AND MAGNETOSTRATIGRAPHY

Biostratigraphy

Calcareous Nannofossils

A calcareous nannofossil range distribution table for Site 1043 in Table 7 shows the distribution with depth of nannofossils within the recovered cores. The top two cores from Site 1043A cannot be biostratigraphically zoned because of the absence of zonal indicator fossils. Sample 170-1043A-1H-CC contains Pliocene to Miocene reworked species and Sample 170-1043A-2H-CC is nearly barren. Samples 170-1043A-3X-CC through 13X-CC (117.4 mbsf) contain

Table 6. Site 1043 structural summary.

Site	Hole	Core	Type	Section	Top (cm)	Bottom (cm)	Depth (mbsf)	Cr az.	Cr dip	Pm az.	Pm dip	Half	Tool	Identifier
1043	A	2	H	2	106	106	10.56	180	88	360	2	W	MMT	Bedd
1043	A	3	X	1	48	48	17.38	208	78	66	30	W	MMT	Bedd
1043	A	3	X	1	78	78	17.68	35	82	104	36	W	MMT	Bedd
1043	A	3	X	1	79	79	17.69	206	86	81	26	W	MMT	Bedd
1043	A	3	X	1	80	80	17.70	9	85	119	10	W	MMT	Bedd
1043	A	3	X	3	5	5	19.95	30	80	109	31	W	MMT	Bedd
1043	A	5	X	3	28	35	36.68			100	50	W	Protr.	Fiss.?
1043	A	5	X	3	75	82	37.15			87	61	W	Protr.	Fiss.?
1043	A	8	X	1	22	22	61.82	340	88	264	20	W	MMT	Bedd
1043	A	8	X	1	22	22	61.82	346	88	262	14	W	MMT	Frac

Notes: Cr az. = core reference azimuth, Cr dip = core reference dip, Pm az. = paleomagnetic azimuth, Pm dip = paleomagnetic dip, Half = core half (W = working half, A = archive half). MMT = tool designed by Martin Mesch, and Protr. = protractor. Bedd. = bedding, Frac = Fracture, and Fiss. = fissility.

This is a sample of the table that appears on the volume CD-ROM.

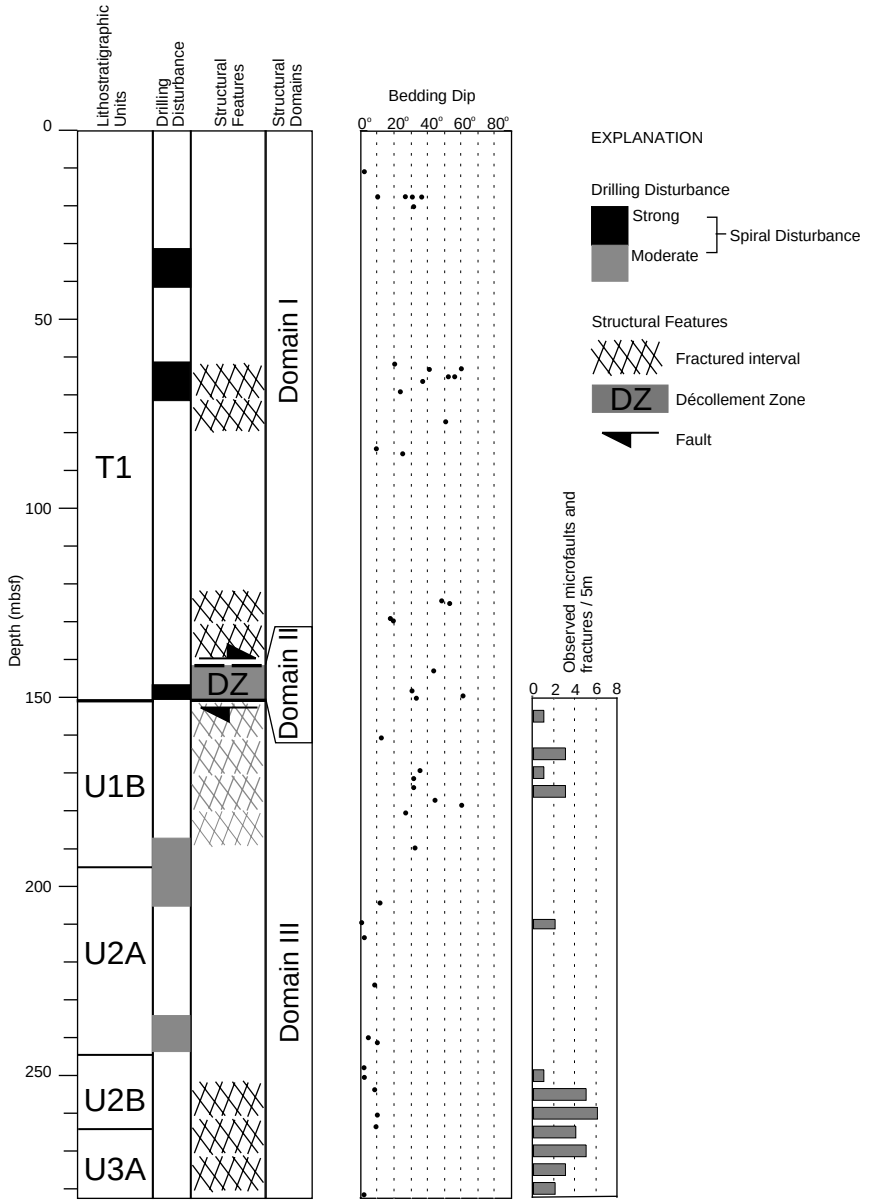

Figure 12. Summary of structural observations at Site 1043.

an assemblage of calcareous nannofossils that are characteristic of early Pleistocene/latest Pliocene Zone NN19. Furthermore, the occurrence of *Helicosphaera sellii* downcore in this interval indicates that these cores are probably older than the last occurrence (LO) datum of *H. sellii* at 1.47 Ma (an equatorial Pacific datum). The observed LO of *Pseudoemiliania lacunosa* (0.46 Ma) and *H. sellii* in Sample 170-1043A-3X-CC indicates a possible thrust fault. Alternatively, reworking is prevalent in this section, and it is possible that *H. sellii* has been reworked upsection.

Samples 170-1043A-14X-CC and 15X-CC (130.5 mbsf) contain poorly preserved assemblages that are characteristic of both late Pleistocene Zone NN20 and early Pleistocene/latest Pliocene Zone NN19. A carbonate clast in the Pleistocene sediments of Sample 170-1043A-15X-1, 24 cm, contains a moderately preserved early Miocene assemblage that is typical of the *Helicosphaera ampliaperta* Zone seen in the Site 1039 underthrust section.

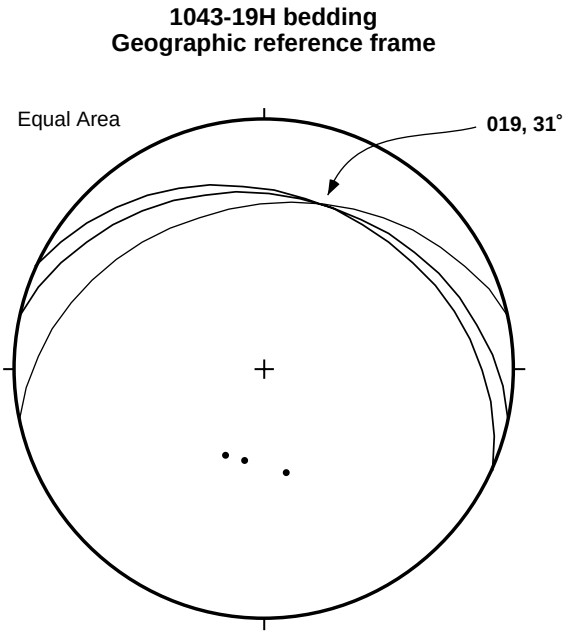

Figure 13. Bedding attitudes from an interval ~20 m below décollement zone, corrected to true geographic coordinates with remanence magnetization data (Core 170-1043A-19H).

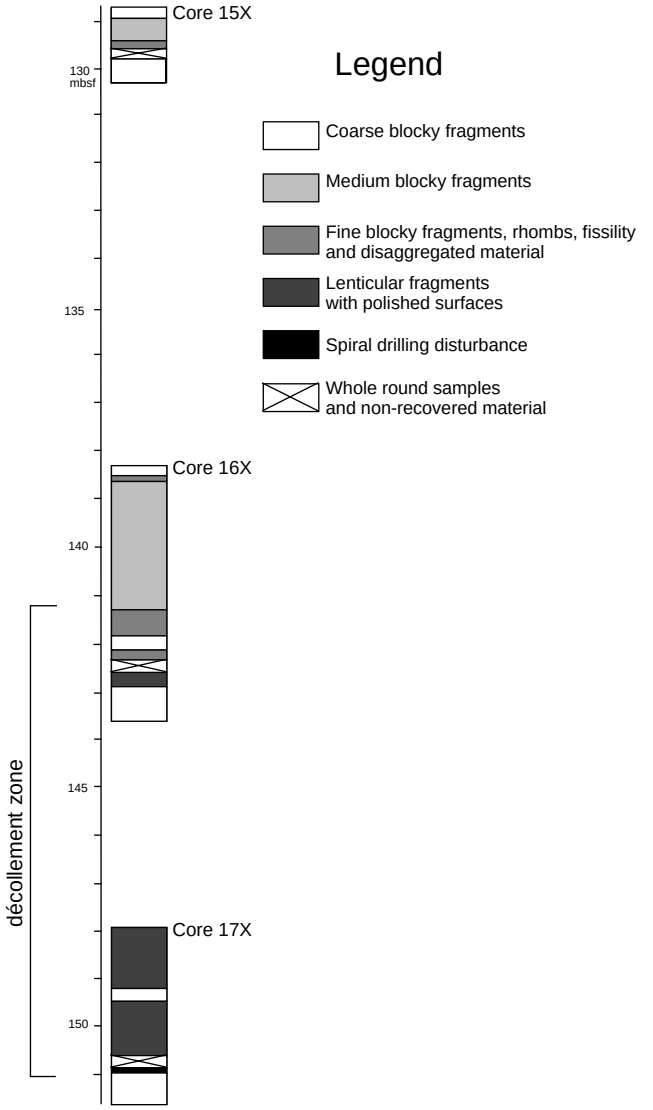

Figure 15. Log of structural features within the décollement zone in Hole 1043A.

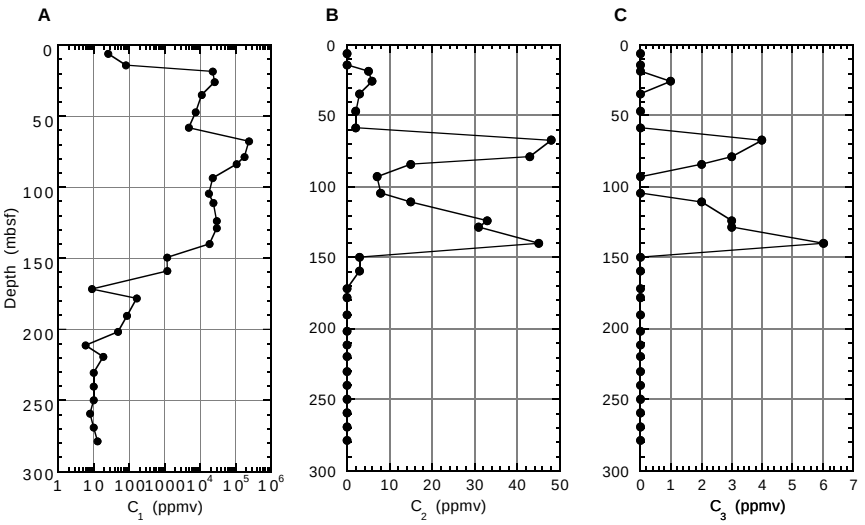

Figure 14. Results of headspace gas analyses for (**A**) methane, (**B**) ethane, and (**C**) propane vs. depth.

Table 7. Calcareous nannofossil range distribution chart for Site 1043.

Calcareous nannofossil zone	Core, section	Depth (mbsf)	Abundance	Preservation	Small reticulofenestrids	*Coccolithus miopelagicus*	*Discoaster berggrenii*	*Discoaster brouweri*	*Discoaster intercalaris*	*Discoaster quinqueramus*	*Reticulofenestra pseudoumbilicus*	*Sphenolithus abies*	*Sphenolithus moriformis*	*Sphenolithus verensis*	*Calcidiscus leptoporus*	*Triquetrorhabdulus rugosus*	*Helicosphaera carteri*	*Pontosphaera discopora*	*Calcidiscus macintyrei*	*Ceratolithus rugosus*	*Discoaster surculus*	*Gephyrocapsa caribbeanica*	*Gephyrocapsa oceanica*	*Helicosphaera sellii*	*Pseudoemiliania lacunosa*	*Coronocyclus nitescens*	*Cyclicargolithus floridanus*	*Discoaster deflandrei*	*Helicosphaera ampliaperta*	*Sphenolithus heteromorphus*	*Helicosphaera wallichii*	*Reticulofenestra asanoi*	*Helicosphaera neogranulata*
	170-1043A-																																
?	1H-CC	7.99	R	M	R								r	r	R																		
	2H-CC	16.89	R	P											R				r														
	3X-CC	21.5	R	G	R																			R	R								
	4X-CC	29.76	A	G	A										C		F	R				C	C	R	F								
	5X-CC	38.93	A	G	A										C		F	C				C			C								F
	6X-CC	48.63	C	M	F										R		F					C	C		F								
NN19	7X-CC	59.68	A	M	C										F		C					C	C		F								R
	8X-CC	69.48	B																														
	9X-CC	80.69	C	M	F												F					C	F		F								
	10X-CC	86.18	C	M	C										R		R					C	F										
	11X-CC	94.82	C	M	C	a					r	f	c	f	R		F					F		R	R								
	12X-CC	109.71	C	M											F			R				C	C		F								
	13X-CC	117.14	C	M	C												F	R				C	C	R							F	R	
NN20-NN19	14X-CC	126.35	C	P											R		F					C	F										
NN 4	15X-1	129.66	A	M		C			F		C		A		R		F	F	R							C	C	F	R	C			
NN20-NN19	15X-CC	130.31	C	P											R		F					C	F										
	16X-CC	144.52	B																														
?	17X-CC	151.81	R	P											R								R										
NN21-NN20	18X-CC	161.52	C	M	R																	R	R										
	19H-CC	176.9	R	P											F								C		F								
	20X-CC	181.89	C	P											F							C	F		C								
	21X-CC	195.13	F	M													F						F		F								
NN19	22X-CC	205.45	F	P	F										F							F		F	F								
	23X-CC	214.47	F	M	F										F							F		F	F								
	24X-CC	224.53	F	M	F										F							F	F	F									
NN18	25X-CC	234.33	F	P					F						F		F	F	R	R													
NN16	26X-CC	241.91	C	M	C				F		C				F		F	F	R	R	F												
NN15-NN14	27X-CC	253.55	C	M	F				F		F	F	F	F	F		F	F															
	28X-CC	263.13	C	G	F		C			C	C	F	F		F	F																	
NN11	29X-CC	272.84	C	G	F	F	F	F	F	F	F																						
	30X-CC	282.26	C	M	C	F	F	F	R	R	C	F	F	F																			

Notes: Abbreviations for abundances are as follows: A = abundant, C = common, F = few, R = rare, B = barren, and lowercase letters = reworked. Abbreviations for preservation are as follows: G = good, M = moderate, and P = poor. For more specific definitions refer to the "Explanatory Notes" chapter (this volume).

This table also appears on the volume CD-ROM.

Sample 170-1043A-16X-CC is barren, and 17X-CC is nearly barren, so a nannofossil zonation determination cannot be made. Samples 170-1043A-18X-CC and 19HH-CC through 24X-CC are late and early Pleistocene, respectively.

The late Pliocene *Discoaster brouwerii* Zone (NN18) is observed in Sample 170-1043A-25X-CC. Zones NN17 and NN16 were not resolved either because of the wide sampling interval, or because of an unconformity located in the interval between these two samples.

Samples 170-1043A-26X-CC and 27X-CC (253.55 mbsf) contain an assemblage of nannofossils representative of either the early Pliocene *Reticulofenestra pseudoumbilica* or *Discoaster asymmetricus* Zones (NN15 and NN14, respectively). The LO's of *R. pseudoumbilica* and the sphenoliths are observed in this interval. No other NN15 or NN14 zonal markers are seen.

The occurrence of *Discoaster berggreni* and/or *Discoaster quinqueramus* assigns Samples 170-1043A-28X-CC through 30X-CC (282 mbsf) to the late Miocene *D. berggreni* Zone (NN11).

Diatoms

Diatoms are variable in abundance and preservation at Site 1043, but show distinctive characteristics above and below the décollement surface. Table 8 shows the abundance and zonal distribution of diatom assemblages from this site.

Diatoms in the silty clays and breccias of the toe of slope unit (T1) are generally rare to absent and poorly preserved (Table 8). In Samples 170-1043A-1H-CC (7.99 mbsf) through 14X-CC (126.35 mbsf), no age-diagnostic taxa are present; therefore diatom zonation of this part of the section is not possible. An exception to this trend of poorly preserved diatoms in Unit T1 is the occurrence of common and moderately preserved diatoms that are characteristic of the late Pleistocene *Pseudoeunotia doliolus* Zone in Sample 170-1043A-15X-CC (130.31 mbsf). Species such as *P. doliolus*, *Thalassiosira oestrupii*, *Azpeitia nodulifer*, and *Nitzschia marina*, without the presence of *Nitzschia reinholdii* or *Nitzschia fossilis*, indicate that this sample is younger than 0.62 Ma (Table 8). Although this age estimate contradicts the nannofossil and foraminifer age estimates for this depth, it is possible that a thin interval of late Pleistocene diatomaceous clay has been faulted into the slope wedge (see "Lithostratigraphy and Structures" section, this chapter). In Sample 170-1043A-16X-CC, the last sample above the décollement that was examined for diatoms, taxa are rare and poorly preserved and contain no age-diagnostic species.

Within Core 170-1043A-17X at ~150 mbsf, the décollement surface is present. Below the décollement, Samples 170-1043A-17X-CC through 20X-CC consist of diatomaceous ooze and clay and are part of lithologic Unit U1B. These samples contain abundant to common diatoms that are characteristic of the late Pleistocene *P. doliolus* Zone (Table 8), which ranges in age from 0 to 0.62 Ma.

Sample 170-1043A-21X-CC (195.13 mbsf) is within the silty clays of lithologic Unit U2A, a unit where diatoms are rare to few and often poorly preserved. However, three samples within this unit have rare occurrences of stratigraphically significant diatoms, suggesting an early Pleistocene to late Pliocene age for Unit U2A. Sample 170-

Table 8. Diatom range distribution chart for Site 1043.

Diatom zone	Core, section	Depth (mbsf)	Abundance	Preservation	*Actinocyclus ellipticus* var. *javanica*	*Actinocyclus moronensis*	*Cestodiscus pulchellus*	*Denticulopsis hustedtii*	*Hemidiscus cuneiformis*	*Nitzschia porteri*	*Thalassionema nitzschioides*	*Thalassiosira yabei*	*Thalassiothrix longissima*	*Azpeitia nodulifer*	*Coscinodiscus lewisianus*	*Nitzschia cylindrica*	*Nitzschia miocenica*	*Rossilla praepaleacea*	*Nitzschia fossilis*	*Thalassiosira oestrupii*	*Nitzschia marina*	*Thalassiosira convexa* var. *aspinosa*	*Rhizosolenia praebergonii* var. *robusta*	*Nitzschia reinholdii*	*Pseudoeunotia doliolus*	*Asteromphalus elegans*	*Actinocyclus ellipticus* f. *lanceolata*	*Actinoptychus senarius*	*Coscinodiscus marginatus*
	170-1043A-																												
	1H-CC	7.99	F	P			r				R		R	R	r					R									R
	2H-CC	16.89	B																										
	3X-CC	21.5	B																										
	4X-CC	29.76	B																										
	5X-CC	38.93	B																										
	6X-CC	48.63	F	P							R		R							R	R		r						
?	7X-CC	59.68	R	P																			r					R	
	8X-CC	69.48	R	P																									
	9X-CC	80.69	B																										
	10X-CC	86.18	R	P							R		R									R							
	11X-CC	94.82	R	P							R		R																
	12X-CC	109.71	R	P				r			R		R	R						R			r						
	13X-CC	117.14	B																										
	14X-CC	126.35	B																										
P. doliolus	15X-CC	130.31	C	M							F		F	R						F	F				R				
?	16X-CC	144.52	R	P							R																		
	17X-CC	151.81	A	M							C		F	F						C	F		r		F	R	r	R	
P. doliolus	18X-CC	161.52	C	M					R		F		R							F	F		r		F	R			
	19H-CC	176.9	C	M							F		R	F						C	F				F				
	20X-CC	181.89	C	P							R		R							F	F				R				
	21X-CC	195.13	F	P							R		R						R	R	R		r		R				
N. reinholdii Sz B	22X-CC	205.45	F	P							F			R					R	F	F		r	R	R				
	23X-CC	214.47	B																										
N. reinholdii Sz A	24X-CC	224.53	R	P							R								R	R	R		R						
N. marina Sz B	25X-CC	234.33	R	P							R		R						R	R	R	R							
N. marina Sz A?	26X-CC	241.91	B																										
	27X-CC	253.55	B																										
?	28X-CC	263.13	F	P							F		F	R					R	F									
T. convexa Sz A	29X-CC	272.84	A	G						R	C		C	F	r	R	R	R											
A. moronensis	30X-CC	282.26	A	G	F	R	r	C	F	R	C	R	A														R		

Notes: Abbreviations for abundances are as follows: A = abundant, C = common, F = few, R = rare, B = barren, and lowercase letters = reworked. Abbreviations for preservation are as follows: G = good, M = moderate, and P = poor. For more specific definitions refer to the "Explanatory Notes" chapter (this volume). Sz = subzone.

This table also appears on the volume CD-ROM.

1043A-21X-CC has rare *N. fossilis* (LO = 0.70 Ma), placing it in the *N. reinholdii* Subzone B. Sample 170-1043A-24X-CC has well-preserved specimens of *Rhizosolenia praebergonii* var. *robusta*, whose LO is 1.72 Ma, which places it at the B/A Subzone boundary in the *N. reinholdii* Zone. Finally, Sample 170-1043A-25X-CC has rare *Thalassiosira convexa* var. *aspinosa* (LO = 2.43 Ma) placing this sample in the late Pliocene *N. marina* Zone (Subzone B/A boundary).

Samples 170-1043A-26X-CC through 28X-CC (Subunits U2A–U2B) are either barren or show rare diatoms, which prevents the clear identification of diatom zones for this interval. However, extrapolation from the age-depth plot (Fig. 16) suggests an early Pliocene to latest Miocene age for these samples.

Samples 170-1043A-29X-CC and 30X-CC are part of Subunit U3A (siliceous nannofossil ooze) and have abundant and well-preserved diatom assemblages, suggesting a late Miocene age for the bottom of Hole 1043A (Table 8). The taxa in Sample 170-1043A-29X-CC are characteristic of the *T. convexa* Zone (Subzone A). In particular, the presence of *Rossiella praepaleacea* (LO = 6.52 Ma) in Sample 29X-CC (272.84 mbsf) supports this age assignment. Sample 170-1043A-30X-CC (282.26 mbsf) has a varied assemblage and includes *Thalassiosira yabei*, *Denticulopsis hustedtii*, and *Actinocyclus moronensis.* The LO of *D. hustedtii* and *A. moronensis* is nearly identical in age, 9.6 and 9.66 Ma, respectively, and defines the upper boundary of the *A. moronensis* Zone (Fig. 17). Although these ages are several million years older than the other biostratigraphic and magnetostratigraphic estimates for this depth, a comparison of the age-depth relationship from the late Miocene at Sites 1039 and 1040 supports slow apparent age-depth rates (6 m/m.y. or possibly slower; Fig. 16), which would allow for the presence of closely spaced datums.

Planktonic Foraminifers

Planktonic foraminifers in samples at Site 1043 range in age from the Pleistocene to the late Miocene (Table 9). Planktonic foraminifers generally are present in all core-catcher samples except Samples 170-1043A-29X-CC and 30X-CC, which are barren. Hole 1043A yields few to rare planktonic foraminifers that are moderate to well preserved. Some planktonic foraminifer zones are recognized, and their zonal assignments are described below.

In the upper part of Hole 1043A, Samples 170-1043-1H-CC through 17X-CC are assigned to the Pleistocene. Sample 170-1043A-1H-CC, which contains *Globorotalia bermudezi* and dextrally coiled *Pulleniatina obliquiloculata,* is younger than 0.74 Ma. In Samples 170-1043A-2H-CC and 3X-CC, Pliocene to Miocene marker planktonic foraminifers are mixed. In Sample 170-1043A-4X-CC, the coiling change in *Pulleniatina* indicates an age of 0.74 Ma. The LO of *Globigerinoides extremus* is recognized in Sample 170-1043A-13R-CC, indicating an age of 1.77 Ma.

The lower part of Hole 1043A ranges in age from Pleistocene to late Miocene. The LO of *Pulleniatina finalis* (1.4 Ma) is in Sample 170-1043A-18X-CC. The LO of *G. extremus* is recognized in Sample 170-1043A-22R-CC, indicating an age of 1.77 Ma. Samples 170-1043A-25X-CC and 26X-CC are assigned to Zone N21 (late

Pliocene), based on occurrence of *Globorotalia tosaensis* and dextrally coiled *P. obliquiloculata*. Sample 170-1043A-27X-CC is assigned to Zones N19 through N21, based on the co-occurrence of *Globorotalia exilis* and *Neogloboquadrina acostaensis.* Sample 170-1043A-28X-CC is assigned to the late Miocene, based on occurrence of *Globorotalia plesiotumida* and *Globorotalia limbata.* Samples 170-1043A-29X-CC and 30X-CC are barren of planktonic foraminifers.

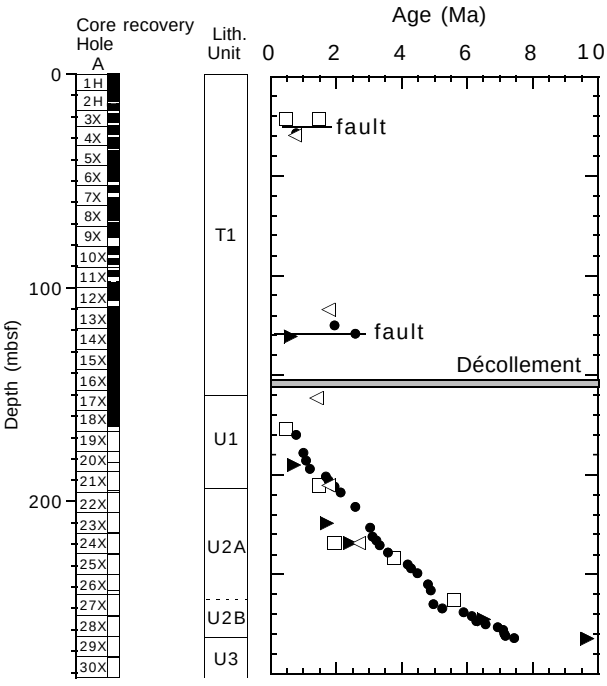

Figure 16. Age-depth correlations of biostratigraphic datums from Site 1043. Calcareous nannofossils = open boxes, diatoms = solid triangles, and planktonic foraminifers = open triangles. Paleomagnetic reversal boundaries = solid circles. Age-depth inversions defining thrust faults at ~25 and 125 mbsf are indicated.

Paleomagnetism

Pass-through measurements of split cores after 20-mT AF demagnetization, and of discrete samples after 40-mT AF demagnetization, were largely successful in defining the magnetostratigraphy at this site. A steep, downward drilling-induced remanence was commonly observed, which required fields of up to 40 mT to remove. Where this overprint is particularly strong, magnetostratigraphy was more reliably constrained by discrete samples. An additional complication to be noted is the disturbance of Core 170-1043A-7X, which was caused by a failed plastic liner. This core was apparently not reassembled correctly, so the reversed intervals within this core should be discounted.

Wedge Sediments

Although a detailed magnetostratigraphy can not be reconstructed within the sediments above the décollement (Fig. 18A), several polarity reversal boundaries can be identified with the aid of biostratigraphic markers. The B/M boundary (0.78 Ma) occurs at 28.5 mbsf, and the onset of Chron C2n (1.95 Ma) occurs at 125 mbsf. A sequence of reversals occurs just above the décollement, indicating that these sediments are older than 0.78 Ma. Immediately below the décollement, sediments are normal polarity.

Underthrust Sediments

With the aid of biostratigraphic markers, a fairly complete magnetostratigraphy has been obtained from the underthrust sediments at this site, with polarity chrons ranging from the B/M boundary (0.78 Ma) at 180 mbsf, to the termination of Chron C4n.1n at 282 mbsf (Fig. 18B). Comparing the depth of the B/M boundary at this site (180 mbsf, 30 m below the décollement) with the depth of this polarity transition at Site 1039 (59 mbsf), indicates that the portion of lithostratigraphic Unit U1 above the B/M boundary has been thinned

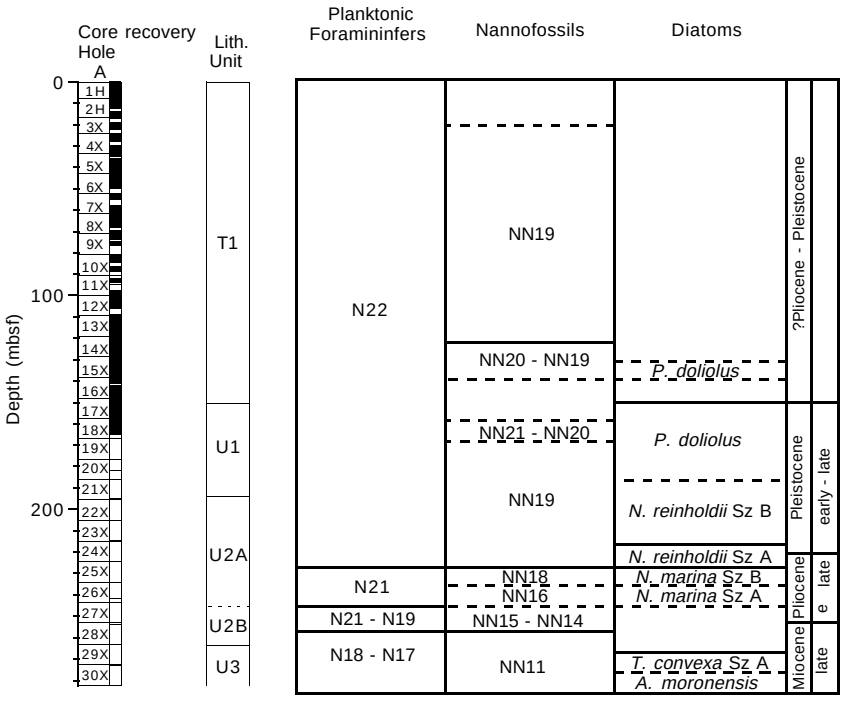

Figure 17. Correlation of the planktonic foraminifer, calcareous nannofossil, and diatom zones with Site 1043 cores and sedimentary units. Dashed lines = uncertainty in placement of the zonal boundary.

Table 9. Planktonic foraminifer range distribution chart for Site 1043.

Planktonic foraminifer zone	Core, section	Depth (mbsf)	Abundance	Preservation	*Candeina nitida*	*Dentoglobigerina altispira*	*Dentoglobigerina globosa*	*Globigerina bulloides*	*Globigerina falconensis*	*Globigerinella aequilateralis*	*Globigerinita glutinata*	*Globigerinoides conglobatus*	*Globigerinoides extremus*	*Globigerinoides immaturus*	*Globigerinoides obliquus*	*Globigerinoides quadrilobatus*	*Globigerinoides ruber*	*Globigerinoides sacculifer*	*Globigerinoides tenellus*	*Globigerinoides trilobus*	*Globoquadrina venzuelana*	*Globorotalia bermudezi*	*Globorotalia crassaformis*	*Globorotalia crassula*	*Globorotalia exilis*	*Globorotalia limbata*	*Globorotalia menardii*	*Globorotalia plesiotumida*	*Globorotalia scitula*	*Globorotalia theyeri*	*Globorotalia tosaensis*	*Globorotalia tumida*	*Globorotalia ungulata*	*Globorotaloides hexagona*	*Neogloboquadrina acostaensis*	*Neogloboquadrina dutertrei*	*Neogloboquadrina humerosa*	*Neogloboquadrina pachyderma*	*Orbulina universa*	*Pulleniatina finalis*	*Pulleniatina obliquiloculata*	*Sphaeroidinella dehiscens*	*Sphaeroidinellopsis seminulina*	*Zeaglobigerina decoraperta*	*Zeaglobigerina rubescens*
	170-1043A-																																										
	1H-CC	7.99	F	G						R						R	R	R	R			R	T				R			R				R			R						
	3X-CC	21.5	R	M							R						R										R				R			R		R						
	4X-CC	29.76	R	G								R					R	R		R							R							R					R			
	5X-CC	38.93	F	G							R						R			R							R				R	R		R					R			
	6X-CC	48.63	R	M													R	R									R										R	R	P			
	7X-CC	59.68	R	M								R					R	R		R							R					R		R					R			R
	8X-CC	69.48	T	M				T																														R				
	9X-CC	80.69	F	M		T											R	R		R							R					R		R					R			
	10X-CC	86.18	R	M								R					R	R						R			R												R		T	
	11X-CC	94.82	R	P						R							R	R		R							R					R							R			
	12X-CC	109.71	R	M								R					R	R																				R				
	13X-CC	117.14	R	M							R		R				R										R					R		R							
N22	14X-CC	126.35	R	M	R						R						R										R							R								
	15X-CC	130.31	R	M													R							T																		
	16X-CC	144.52	R	M									R	R			R	R									R															
	17X-CC	151.81	R	M										R			R										R					R										
	18X-CC	161.52	R	G								R					R	R									F				R	R	R						R	R		
	19H-CC	176.9	R	G					R								R	R								R			R						R	R					R	
	20X-CC	181.89	F	M												R	R	R								R			R			R	R		R					R		
	21X-CC	195.13	F	G							R					R	R	R	R		R					R						R		R		R	R			R		
	22X-CC	205.45	R	M	R						R		R		R		R	R			R						F					R				R	R		R		R		
	23X-CC	214.47	R	G							R						R										R									R						
	24X-CC	224.53	R	P													R										R													T		
N21	25X-CC	234.33	R	M													R	R									R					R	R			R				R		
	26X-CC	241.91	F	M			R						R		R		R				R					R	R							R	R					R		
N21-N19	27X-CC	253.55	R	M							R				R						R					R	R							R	R					R		
	28X-CC	263.13	C	M									R		R		R	R			R	R				R		R													R	
N17-N18	29X-CC	272.84	B																																							
	30X-CC	282.26	B																																							

Notes: Abbreviations for individual species abundances are as follows: A = abundant, C = common, F = few, R = rare, T = trace, and B = barren. Abbreviations for preservation are as follows: G = good, M = moderate, and P = poor. For more specific definitions refer to the "Explanatory Notes" chapter (this volume).

This table also appears on the volume CD-ROM.

~30 m by some combination of faulting and/or compaction at this site.

Age-Depth Correlation

Within the wedge sediments, reversals in age-depth distribution can be used to define the occurrence of thrust faults. A foraminifer marker with an age of 1.77 Ma in Core 170-1043A-13X, the Chron C2n onset at 125 mbsf, and the occurrence of a diatom marker with an age less than 0.62 Ma in Core 170-1043A-15X, indicates that an age-inversion occurs between 125 and 130 mbsf, arguing strongly for the existence of a thrust fault within this interval. Another possible age-depth inversion defined by nannofossil and foraminifer datums and the B/M magnetic polarity boundary (see Table 10) occurs between Cores 170-1043A-2H and 170-1043A-3X, matching an interval of low density, high porosity at 25–30 mbsf in the LWD logs of Hole 1043B (see "Physical Properties" section, this chapter).

Mixed polarity sediments from above the décollement and normal polarity (Brunhes) sediments immediately below the décollement at 150 mbsf also indicate the occurrence of an age reversal at this fault.

Below the décollement, age-depth relationships can be calculated using a combination of biostratigraphic and paleomagnetic information (Table 10; Fig. 16). Within Unit U1 (150–195.45 mbsf), age-depth relationships range from 52 m/m.y., which is defined by biostratigraphic markers, to 40 m/m.y., which is defined by magnetostratigraphy. Age-depth relationships for both biostratigraphy and magnetostratigraphy are 15 m/m.y. within Unit U2 (195.45–263 mbsf) and 12 m/m.y. within Unit U3 (263 mbsf to TD).

GEOCHEMISTRY

Overview

The main geochemical objectives at this site, located about 1.3 km west of Site 1040 and closer to the deformation front, are the same as for Site 1040 (see "Geochemistry" section, "Site 1040" chapter, this volume), with particular emphasis on off-scraping.

As at Site 1040, the chemical compositions of the volatile hydrocarbons and pore fluids are distinctly different in the wedge and underthrust sections, with a less sharp transition at the base of the décollement zone at ~150 mbsf. Methane (C_1), ethane (C_2), and propane (C_3) are present in the wedge, indicating the presence of a thermogenic fluid component with concentration maxima at 18–26, 68–84, and 120–145 mbsf. Background levels of methane concentrations were observed in the underthrust section; ethane and propane are absent. Three C_1–C_3 maxima are also present in the wedge section of Site 1040, and at both sites they occur at depth intervals of faults acting as fluid conduits. Fluid flow is indicated by distinct C_1 concentration maxima accompanied by concentration minima or maxima of other major and minor components and is clearly recorded on the LWD logs and in the core physical properties, especially, by sharp decreases in porosity and increases in grain density (see "Physical Properties" section, this chapter). The deepest of the three hydrocarbon concentration maxima is at the base of the décollement zone, where the Cl concentration is 9.5% lower than that of seawater; at Site 1040, Cl at the décollement is diluted by 13%.

Across the décollement zone, the shifts in the chemical and physical properties are less extreme at this site than at Site 1040, and in

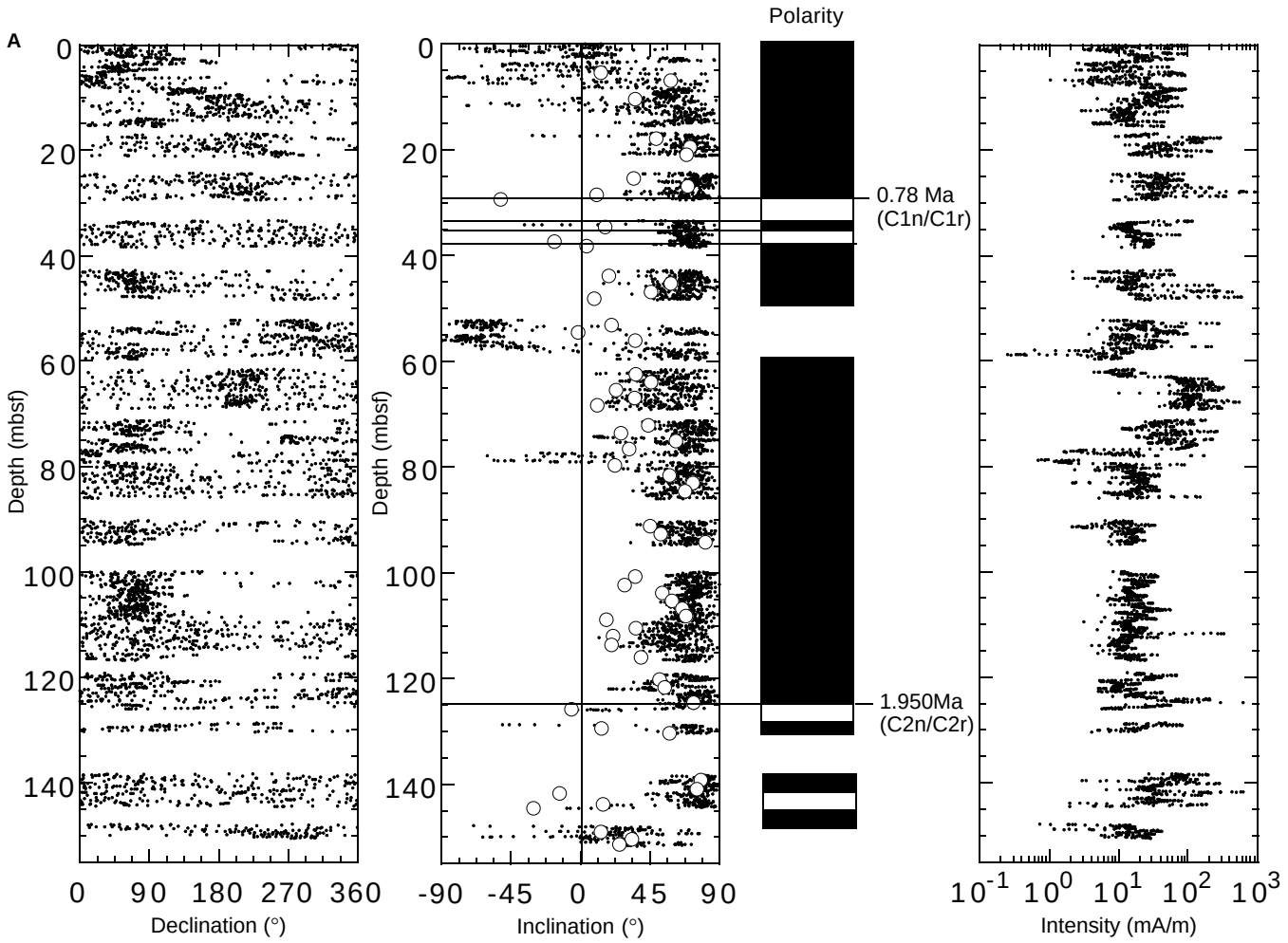

Figure 18. **A.** Pass-through, split-core remanence results after 20-mT AF demagnetization, and discrete sample results after 40-mT AF demagnetization from Hole 1043A, 0–150 mbsf. **B.** Pass-through, split-core remanence results after 20-mT AF demagnetization, and discrete sample results after 40-mT AF demagnetization from Hole 1043A, 150 mbsf to TD.

some components the direction of shift is reversed. At this site, salinity increases by 2 below the décollement whereas at Site 1040, the salinity increases by 5, from 29 to 34. Chlorinity is higher by only 1–2 mM below the décollement at this site, whereas at Site 1040 it is higher by ~35 mM. Ca concentrations are higher by about 4 mM below the décollement at this site, whereas at Site 1040 they are lower by about 17 mM. Phosphate concentrations are practically zero at and above the décollement at Site 1040, whereas at Site 1043 phosphate concentration maxima occur both immediately above and below the décollement zone. Similar differences between the sites are observed for each component. Furthermore, at Site 1040 below the fluid conduit at 180–200 mbsf, the pore fluids of the lower wedge section are chemically distinct from those of the upper wedge section. They are strongly influenced by the deep-seated fluid that carries the propane, and they are characterized by having significantly higher Ca concentrations and lower Mg, K, and Si concentrations than the fluid immediately above the conduit. At this site, however, the pore-fluid chemistry below and above the fluid conduit at 65–80 mbsf is much less distinct or reversed in direction. For example, there is no change in the Ca concentration across it; Mg concentrations are higher below the conduit at this site but lower below the conduit at Site 1040, and a similar reversed trend is seen in the Si and K concentrations. All these pronounced chemical changes across the décollement and the shallower conspicuous fluid conduit in the wedge can be attributed to mixing between the lower wedge and uppermost hemipelagic pore fluids. This pore-fluid mixing could be achieved by advection of fluid from the underthrust section across the décollement and into the lower wedge, or by offscraping of the uppermost hemipelagic sediments and/or imbrication in the lower wedge. The available chemical data, together with additional shore-based data, including pore-fluid isotope ratios and XRF geochemistry of the sediments, will provide an excellent base for distinguishing between these explanations for the pore-fluid profiles.

The inorganic and organic carbon and sulfur contents of the sediments at this site are similar to those at Site 1040. Because the differences in concentrations above and below the décollement are small (not withstanding the inorganic carbon content of the underthrust calcareous section), the off-scraping process is not evident from these data. Sediment XRF analyses for this site were not conducted aboard ship because of time constraints.

Gas Results

Volatile Hydrocarbons

Volatile gas results are displayed in Table 11 and Figure 14. Methane concentrations in the headspace volumes range between 26 and 116,561 ppmv. The C_1 concentration profile shows three distinct patterns. In the uppermost part of the sedimentary sequence, methane concentrations increase from 26 ppmv at 6.03 mbsf to 23,060 ppmv at 18.4 mbsf (Fig. 14A). Between 18.4 and 139.8 mbsf, generally

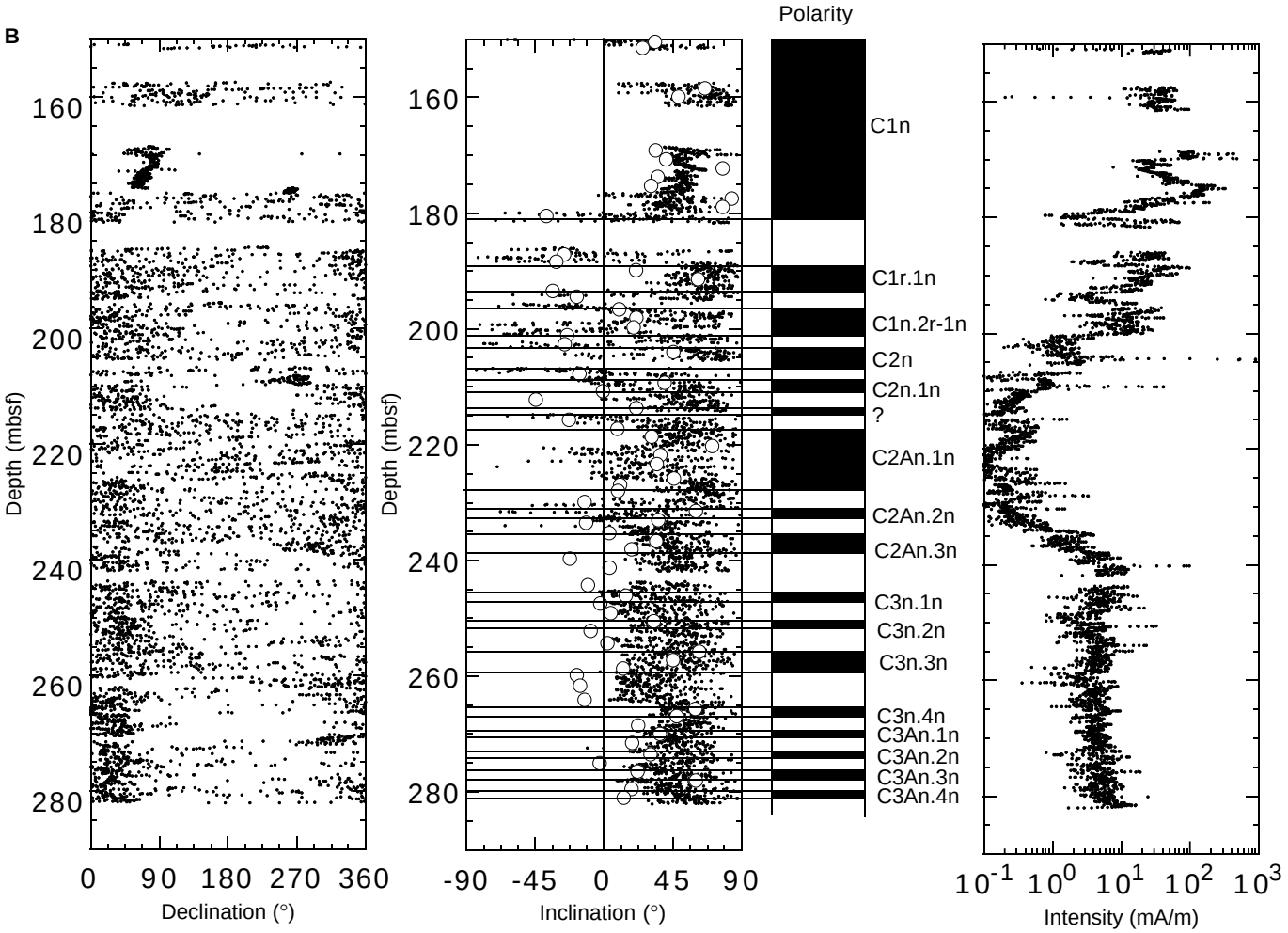

Figure 18 (continued).

high concentrations ranging from 4,770 to 237,615 ppmv were detected. Below the base of the décollement (see "Lithostratigraphy and Structures" section, this chapter) methane decreases considerably to 10 ppmv and remains low throughout the whole underthrust section. The downhole profiles for ethane and propane measured by the headspace technique are shown in Figures 14B and 14C, respectively. Both compounds are absent in the first two cores of Hole 1043A. Ethane was first detected at a depth of 18.4 mbsf. Ethane concentrations show a maximum of 48 ppmv at 67.6 mbsf. Below this depth, the ethane concentrations decrease and vary between 7 and 45 ppmv. In the subducted sediments, ethane is absent. Propane concentrations are generally low. Between 67.6 and 139.8 mbsf only small amounts of propane (2–6 ppmv) were measured. This zone of higher propane concentration is characterized by three concentration maxima, suggesting an admixture of allochthonous thermogenic gas. Below 139.8 mbsf, propane is absent throughout the whole underthrust section.

Pore-Water Results

Chloride and Salinity

The most distinctive features of the dissolved chloride and salinity concentration depth profiles (Fig. 19; Table 12) are (1) the three minima, at the décollement and at ~65–80 mbsf, with a lesser one at ~15 mbsf, and (2) the generally step-wise increases in chlorinity and salinity with depth, having lowest values in the upper section of the wedge and highest values in the underthrust section. The possible origins of the low chloride and salinity values at the shallower vs. the deeper wedge sections have been discussed in the "Geochemistry" sections of the "Site 1040" and "Site 1041" chapters (this volume). In summary, in the shallower section the low-Cl signature is either an artifact of gas hydrate dissociation and/or of meteoric water flow, and the deeper section is affected by a low-chloride fluid from greater depth.

Sodium and Potassium

The Na/Cl values and K concentrations show similar differences between the wedge and underthrust sections as the chloride and salinity. The peak of Na/Cl at the décollement is opposite to that at the shallower (~70 mbsf) depth conduit, seen in Figure 20A. Elevated values above the décollement are most likely a result of the above mentioned fluid mixing. No reversal of peak direction is seen in the K concentration at the décollement relative to the shallower conduit (Fig. 20B); the mixing with the hemipelagic fluid, however, reversed the concentration depth sequence of K across the fluid conduit at ~70 mbsf relative to that at Site 1040.

Sulfate, Alkalinity, Ammonium, and Phosphate

The steep sulfate concentration gradient reaches zero at ~20 mbsf in the wedge section (Fig. 21A), the depth where methane concentrations increase (Fig. 14A). Immediately below the décollement, sulfate concentrations increase with depth in the underthrust sediments, at first steeply and then gradually. Thus, methane concentrations are

Table 10. Depths of biostratigraphic and magnetostratigraphic datums observed in Hole 1043A cores.

Depth (mbsf)	Nannofossils (Ma)	Diatoms (Ma)	Paleomagnetic datums (Ma)	Foraminifers (Ma)
21.5				
28.50			0.780	
29.76				0.74
117.14				1.77
125.00			1.950	
129.30			2.580	
130.50		0.62		
161.52				1.40
176.90	0.46			
180.00			0.780	
189.00			0.990	
193.00			1.070	
195.13		0.70		
197.00			1.200	
201.00			1.680	
203.00			1.770	
205.45	1.47			1.77
206.00			1.950	
209.00			2.140	
216.00			2.580	
224.53		1.72		
226.50			3.040	
231.00			3.110	
233.00			3.220	
234.33	1.95	2.43		2.70
235.50			3.330	
239.00			3.580	
241.91	3.75			
245.00			4.180	
247.00			4.290	
249.50			4.480	
255.00			4.800	
258.00			4.890	
263.13	5.60			
265.00			4.980	
267.00			5.230	
269.00			5.894	
271.00			6.137	
272.84		6.52		
273.50			6.269	
275.00			6.567	
276.50			6.935	
278.00			7.091	
280.00			7.135	
281.00			7.170	
282.00			7.432	
282.26		9.66		

Table 11. Composition of headspace gases at Site 1043.

Core, section, interval (cm)	Depth (mbsf)	C_1 (ppmv)	C_2 (ppmv)	C_3 (ppmv)	C_1/C_2
170-1043A-					
1H-5, 0-5	6.03	26	0	0	ND
2H-5, 0-5	14.03	81	0	0	ND
3X-2, 0-5	18.43	23,060	5	0	4,612
4X-2, 0-5	25.93	25,422	6	1	4,237
5X-2, 0-5	34.93	11,009	3	0	3,670
6X-4, 0-5	47.33	7,530	2	0	3,765
7X-5, 0-5	58.23	4,770	2	0	2,385
8X-5, 0-5	67.63	237,615	48	4	4,950
9X-6, 0-5	78.73	175,028	43	3	4,070
10X-3, 0-5	83.73	106,003	15	2	7,067
11X-3, 0-5	93.33	23,069	7	0	3,296
12X-4, 0-5	104.43	17,604	8	0	2,201
13X-2, 0-5	111.03	23,867	15	2	1,591
14X-4, 0-5	123.73	29,387	33	3	891
15X-1, 0-5	128.73	29,323	31	3	946
16X-2, 0-5	139.83	18,394	45	6	409
17X-2, 0-5	149.43	1,185	3	0	395
18X-2, 0-5	159.03	1,201	3	0	400
19X-4, 0-5	171.63	9	0	0	ND
20X-2, 0-5	178.13	165	0	0	ND
21X-4, 0-5	190.53	89	0	0	ND
22X-5, 0-5	201.63	49	0	0	ND
23X-5, 0-5	211.23	6	0	0	ND
24X-4, 0-5	219.33	19	0	0	ND
25X-5, 0-5	230.53	10	0	0	ND
26X-5, 0-5	240.13	10	0	0	ND
27X-5, 0-5	249.73	10	0	0	ND
28X-5, 0-5	259.33	8	0	0	ND
29X-5, 0-5	269.03	10	0	0	ND
30X-5, 0-5	278.63	13	0	0	ND

Notes: C_1, C_2, and C_3 represent methane, ethane, and propane, respectively. ND = not determined. ppmv = parts per million by volume.

This table also appears on the volume CD-ROM.

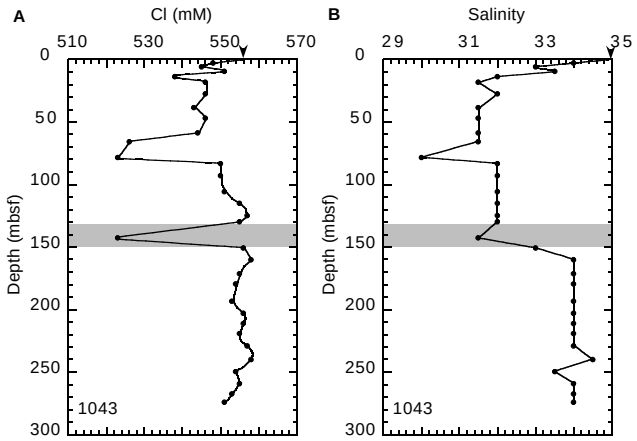

Figure 19. Concentration depth profiles of (**A**) Cl and (**B**) salinity. Arrows = seawater concentration.

high throughout most of the wedge section, and occur at only background levels beneath the décollement. This site is located close to the deformation front where the external supply of dissolved sulfate has ceased to exist, and the remaining internal supply of sulfate at the top of the section has been mostly depleted by bacteria. The bacteria produced an alkalinity that increased by about 5 mM at the top of the underthrust section (Fig. 21B) relative to the maximum concentration at Site 1039. Unlike Site 1040, where alkalinity values are low (~5 mM) in the lower wedge section at and immediately above the décollement, alkalinity values at Site 1043 are high (~19 mM) in the lower wedge section, most likely as a result of mixing with the high alkalinity pore fluids that are characteristic of the uppermost hemipelagic section at Site 1040. Most interesting is the phosphate concentration depth profile (Fig. 21D), which has a distinct concentration maximum of similar magnitude on each side of the décollement zone.

Calcium, Magnesium, and Silica

The Ca, Mg, and Si concentrations in Figure 22 provide insights into the mixing process between the hemipelagic and lower wedge sediments at Site 1043. Ca concentrations in the wedge pore fluids are lower than in seawater at Site 1043 and remain constant from ~20 mbsf to the décollement zone. In most of the underthrust section, the concentrations are somewhat higher than in seawater (Fig. 22A), as at Sites 1039 and 1040. The major and conspicuous difference between the dissolved Ca profiles at Sites 1043 and 1040 is the lack of evidence for the high-Ca, deep-seated fluid in the lower part of the wedge section at Site 1043 and its clear presence at Site 1040. Unlike Ca, dissolved Mg concentrations are distinct in the lower and upper parts of the wedge (Fig. 22B). At Site 1043, the Mg concentrations are higher in the lower part of the wedge than in the upper part, whereas at Site 1040 Mg concentrations are lower in the lower part. This distribution of Mg at Site 1043 can be explained by mixing two components of pore waters found at Site 1040. The mixing is between pore fluids from the uppermost few meters of the hemipelagic sediment section at Site 1040 (Mg concentrations of 47–49 mM—close to seawater) with some pore fluid from the lower wedge sediments at the same site (Mg concentrations of 18–20 mM Mg) at a ratio of 2:1, thus producing the Mg concentration of ~38 mM observed at Site 1043 immediately above the décollement (Fig. 22B).

Table 12. Pore-water chemical data of major and minor constituents, Site 1043.

Core, section, interval (cm)	Depth (mbsf)	Volume (cm^3)	pH	Alkalinity (mM)	Salinity	Cl (mM)	SO_4 (mM)	Mg (mM)	Ca (mM)	K (mM)	Na (mM)	Si (µM)	NH_4 (µM)	PO_4 (µM)	Na/Cl	Mg/Ca
170-1043A-																
1H-2, 140-150	2.90	32	7.77	4.09	34.00	548	25.6	49.2	10.0	11.9	469	565	343	7.5	0.86	4.94
1H-4, 140-150	5.90	32	7.76	13.298	33.00	545	24.9	45.9	7.5	11.0	477	715	976	41.3	0.88	6.15
2H-1, 140-150	9.40	60	7.71	18.225	33.50	551	12.7	45.9	7.7	11.0	458	790	1831	44.5	0.83	5.96
2H-4, 135-150	13.85	18	7.79	19.983	32.00	538	10.5	44.7	5.5	9.9	449	612	2170	26.8	0.83	8.13
3X-1, 120-150	18.10	24	7.79	20.831	31.50	546	1.2	42.5	4.7	9.6	444	470	3552	42.9	0.81	9.04
4X-3, 0-30	27.40	22	8.05	20.747	32.00	546	0.0	36.7	5.0	10.1	453	488	6128	34.0	0.83	7.39
5X-4, 52-87	38.42	20	8.13	20.163	31.50	543	0.0	34.8	5.2	9.9	453	414	12464	28.8	0.83	6.70
6X-3, 115-150	46.95	11	ND	ND	31.50	546	0.0	35.4	5.9	9.6	454	544	15844	33.6	0.83	5.96
7X-5, 65-90	58.64	20	8.09	21.324	31.50	544	0.0	33.5	5.6	9.9	456	542	13283	22.4	0.84	5.93
8X-3, 115-150	65.75	5	ND	ND	31.50	526	0.0	37.1	6.2	9.1	430	398	6402	ND	0.82	6.00
9X-5, 115-150	78.35	12	7.99	18.404	30.00	523	0.0	38.7	5.1	8.9	427	430	4836	18.4	0.82	7.58
10X-2, 115-150	83.35	26	8.07	20.257	32.00	550	0.0	41.5	4.6	9.5	448	574	4158	ND	0.82	9.02
11X-2, 115-150	92.95	29	7.92	21.162	32.00	550	0.0	40.6	4.6	11.0	449	695	3298	31.6	0.82	8.82
12X-4, 115-150	105.55	23	8.00	16.332	32.00	551	0.0	40.6	4.7	10.3	450	727	3151	43.3	0.82	8.67
13X-4, 90-125	114.90	28	7.94	19.15	32.00	555	0.0	38.0	5.1	11.3	457	797	4006	68.6	0.82	7.44
14X-4, 115-150	124.85	31	8.02	18.84	32.00	557	0.0	37.5	5.2	11.4	460	715	4314	42.5	0.83	7.21
15X-1, 96-116	129.66	34	ND	ND	32.00	555	0.0	37.3	5.1	10.3	460	821	3868	34.4	0.83	7.33
16X-3, 115-150	142.45	10	ND	ND	31.50	523	0.0	44.2	4.5	8.8	417	452	3298	11.6	0.80	9.92
17X-2, 115-150	150.55	20	7.99	24.35	33.00	556	4.8	45.9	6.5	9.8	451	740	2189	60.5	0.81	7.07
18X-2, 115-150	160.15	55	7.79	13.668	34.00	558	16.2	45.3	9.5	11.7	469	914	1120	27.6	0.84	4.74
19H-3, 95-120	171.05	50	7.76	14.694	34.00	555	16.1	44.2	9.7	12.2	467	878	1188	24.8	0.84	4.54
20X-2, 130-150	179.40	55	7.95	12.931	34.00	554	16.2	44.9	10.0	11.3	465	932	1171	17.2	0.84	4.48
21X-5, 130-150	193.30	55	7.88	12.434	34.00	553	16.9	43.4	10.4	11.7	467	835	1111	14.0	0.85	4.15
22X-5, 130-150	202.90	50	7.80	10.262	34.00	556	16.6	42.9	11.2	12.0	469	864	1037	14.4	0.84	3.83
23X-4, 130-150	211.00	50	7.89	12.278	34.00	556	17.2	41.7	12.0	12.2	471	855	913	15.6	0.85	3.47
24X-3, 125-150	219.05	42	7.77	11.051	34.00	555	18.5	43.3	12.9	10.7	469	857	780	15.2	0.85	3.37
25X-3, 125-150	228.75	41	7.77	8.86	34.00	557	18.4	42.0	12.7	11.8	473	891	794	7.9	0.85	3.31
26X-4, 125-150	239.85	55	8.04	7.55	34.50	558	19.2	41.2	13.2	12.1	476	770	747	5.5	0.85	3.13
27X-4, 125-150	249.45	36	7.92	6.22	33.50	554	19.5	42.4	13.4	11.0	471	725	589	3.9	0.85	3.18
28X-4, 125-150	259.05	39	7.84	4.13	34.00	555	20.9	42.2	12.8	12.3	475	929	569	2.7	0.85	3.29
29X-3, 125-150	267.25	32	7.64	3.19	34.00	553	21.5	43.0	13.1	12.0	472	1064	561	1.9	0.85	3.29
30X-1, 120-150	273.80	55	7.55	2.78	34.00	551	21.5	42.4	14.3	11.9	469	1062	519	1.5	0.85	2.97

Note: ND = not determined.

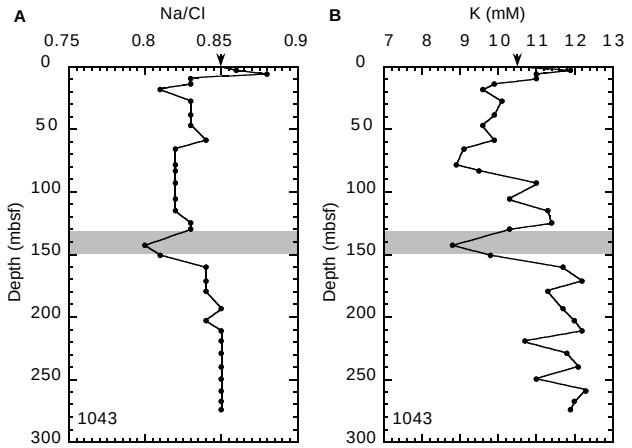

Figure 20. Concentration depth profiles of (**A**) Na/Cl and (**B**) K. Arrows = seawater concentration.

The silica values at Site 1043 can be explained with the same mixing model, using a mixing ratio of 2:1 between the pore fluids of the upper hemipelagic sediments (with silica concentration of ~1000 µM) and the lower wedge sediment (with silica concentration of ~100 µM) at Site 1040, producing the observed silica concentration of ~750 µM above the décollement at Site 1043 (Fig. 22D).

Sediment Results

Inorganic Carbon, Organic Carbon, and Total Sulfur

The results of inorganic and organic carbon, calcium carbonate ($CaCO_3$), nitrogen, and sulfur analyses in the sediments from Hole 1043A are presented in Table 13 and Figure 23. Sediments were generally analyzed at a frequency of three samples per core. Percentages of $CaCO_3$ were calculated from the inorganic carbon concentrations, assuming that all of the carbonates are present as pure calcite. $CaCO_3$

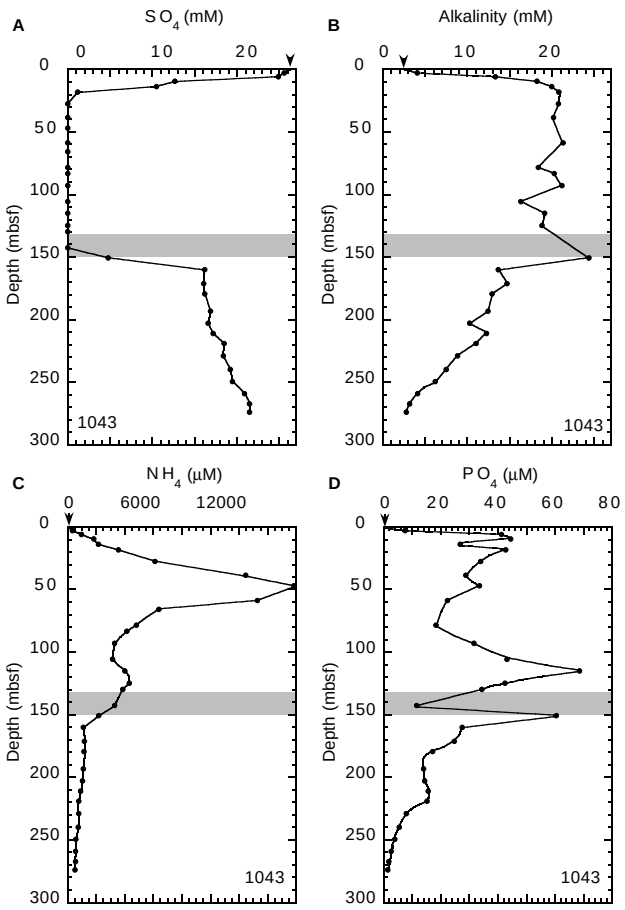

Figure 21. Concentration depth profiles of (**A**) sulfate, (**B**) alkalinity, (**C**) ammonium, and (**D**) phosphate. Arrows = seawater concentration.

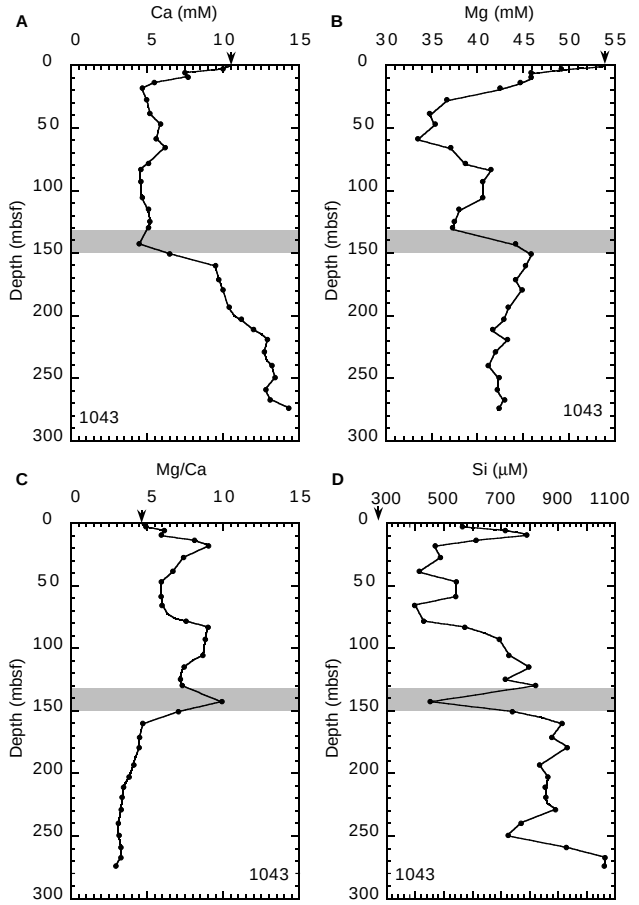

Figure 22. Concentration depth profiles of (**A**) Ca, (**B**) Mg, (**C**) Mg/Ca, and (**D**) silica. Arrows = seawater concentration.

contents are characterized by moderate variations. With the exception of Sample 170-1043-17X-2, 113–114 cm, which contains 11.8 wt% carbonate, $CaCO_3$ concentrations range from 0.7 to 7.8 wt% in the whole sedimentary sequence. Total organic carbon (TOC) contents range from 0.3 to 2.1 wt% (Table 13; Fig. 23B). Above the décollement, TOC fluctuates between 0.8 and 1.4 wt%. In the hemipelagic underthrust sediments (150.5–238.9 mbsf), TOC varies between 0.3 and 2.1 wt%. Total sulfur (TS) concentrations in the hemipelagic sediments at Site 1043 vary between 0.2 and 1.9 wt% (Fig. 23C; Table 12). High sulfur concentrations probably reflect disseminated pyrite and pyrite nodules that are present in the core (see "Lithostratigraphy and Structures" section, this chapter). Total nitrogen (TN) contents vary between 0.09 and 0.23 wt%, with an average value of 0.13 wt% (Table 13).

PHYSICAL PROPERTIES

Density and Porosity

Laboratory Measurements on Cores

Good core recovery and high quality of both APC- and XCB-recovered material enabled a transect of density and porosity to be collected at high sampling rates throughout the section. The gamma-ray attenuation (GRA) densities (Table 14) show the same major trends as densities measured on discrete core specimen measurements (Table 15), although the GRA data are offset to lower values by an almost constant amount because of incomplete filling of the liner and drilling disturbance (Fig. 1). One APC core was taken immediately below the décollement horizon (Core 170-1043A-19H) and, apart from the first section, was found to be almost completely undisturbed. The offset between values from APC and XCB cores (Cores 170-1043A-18X and 20X) in both the GRA and discrete sample data is illustrated clearly. There is a shift of ~0.2 g/cm^3 in the GRA measurements, but less than 0.1 g/cm^3 for the discrete samples, which are selected from the most intact biscuits in the XCB split cores. Values from the APC core are very close to the in situ values determined at the same position from the LWD in the adjacent Hole 1043B (see below). This comparison would suggest that the wet bulk densities measured on discrete samples from the XCB-recovered sediment are systematically lower than true values by ~0.1–0.2 g/cm^3, whereas measured porosities are perhaps 2–4 percentage points higher than the true values.

The upper part of the recovered interval consists of breccias, with firm lumps of claystone, siltstone, and ooze embedded in a clayey to sandy matrix. Although some discrete measurements were made on both matrix and individual clasts, most samples necessarily include an admixture of both, and so the density and porosities for the first 25 m show a wide scatter. It is possible, within this variation, to define a trend of rapidly decreasing porosity from over 75% at the seafloor to ~55% at 20 mbsf. In contrast, clasts from within the breccias have porosities as low as 45%–50%. The wet bulk densities of the clasts are similar (1.6–1.8 g/cm^3) to the densities of the sediment a few tens of meters below. Grain densities in this upper part are also somewhat lower in the matrix than in the clasts, whose grain densities match those of the sediment below. This may indicate that submarine erosion and redeposition may have cut a short way into the wedge and that the debris flows of Unit T1 may have nearby sources.

Between 25 and 50 mbsf, a trend of decreasing porosity is observed (from ~60% to 50%), but the wet bulk density is almost constant over the same interval (1.75 g/cm^3). From 50 mbsf to the décollement (identified at 150.6 mbsf, see "Lithostratigraphy and Structures" section, this chapter), bulk density shows a small but steady decrease that is matched by an increase in porosity from an average of ~48% at 50 mbsf to an average of nearly 56% at 140 mbsf. Two low-porosity/high-density specimens at 143 mbsf were taken from an ash layer that is a minor lithology within the section: this layer shows as a spike on the GRA bulk density record (Fig. 1). Grain densities in this interval are constant at about 2.6 g/cm^3.

Within the décollement zone itself, steep gradients occur in physical properties. Porosity in the prism section (144–150 mbsf) increases slightly downward and, at the boundary itself, increases more rapidly to a value of nearly 70% at 153 mbsf. Wet bulk density reflects this change, decreasing from 1.7 to 1.55 g/cm^3 over the same interval. This pattern suggests that the underthrust sediment immediately below the décollement the has undergone considerable shear-enhanced compaction and that this effect drops off rapidly with distance from the major plane of slip.

Wet bulk density beneath the décollement remains constant to ~210 mbsf before decreasing progressively for the remainder of the recovered interval. The steeper decrease in bulk density at the very bottom of the hole is caused by the lower grain densities, which are best explained by an increase in biogenic silica. Porosity shows an equivalent increase from ~67% at 210 mbsf, to nearly 80% at 280 mbsf (Figs. 1, 24).

Downhole Measurements from LWD

In situ density and porosity measurements were collected by the CDN as part of the LWD downhole assembly. The results are shown in Figures 24 and 25 (see also Table 16). Downhole measurements correlate closely with core measurements (Fig. 1), although downhole densities are significantly lower and porosities are significantly higher than the core-based values in the interval 90–105 mbsf. This can be partly explained by fracturing in this interval (see "Lithostratigraphy and Structures" section, this chapter). Laboratory mea-

Table 13. Inorganic carbon, calcium carbonate, total carbon, total organic carbon, total nitrogen, total sulfur, and TOC/TN in sediments at Site 1043.

Core, section, interval (cm)	Depth (mbsf)	IC (wt%)	$CaCO_3$ (wt%)	TC (wt%)	TOC (wt%)	TN (wt%)	TS (wt%)	TOC/TN
170-1043A-								
1H-2, 138-139	2.88	0.41	3.4	1.26	0.85	0.12	0.31	7
1H-4, 138-139	5.88	0.07	0.6	0.99	0.92	0.15	0.33	6
2H-1, 139-140	9.39	0.07	0.6	0.92	0.85	0.15	1.00	6
2H-4, 134-135	13.84	0.51	4.2	ND	ND	ND	ND	ND
2H-6, 34-35	15.84	0.82	6.9	1.66	0.84	0.12	0.70	7
3X-1, 119-120	18.09	0.47	3.9	1.46	0.99	0.13	1.06	8
4X-2, 33-34	26.23	0.44	3.6	1.44	1.00	0.16	0.60	6
5X-2, 33-34	35.23	0.58	4.8	ND	ND	ND	ND	ND
5X-4, 36-37	38.26	0.38	3.2	1.58	1.20	0.20	0.73	6
6X-3, 114-115	46.63	0.50	4.2	1.89	1.39	0.19	0.41	7
7X-2, 34-35	53.95	0.46	3.9	ND	ND	ND	ND	ND
7X-4, 33-34	56.82	0.94	7.8	2.12	1.18	0.19	0.51	6
8X-3, 114-115	65.74	0.82	6.8	2.18	1.36	0.20	0.22	7
8X-6, 33-34	68.98	0.55	4.6	ND	ND	ND	ND	ND
9X-2, 34-35	73.04	0.87	7.2	ND	ND	ND	ND	ND
9X-5, 88-89	78.08	0.43	3.6	1.66	1.23	0.19	0.35	6
10X-2, 117-118	83.37	0.34	2.8	ND	ND	ND	ND	ND
10X-4, 32-33	85.52	0.80	6.6	2.04	1.24	0.17	1.16	7
11X-2, 112-113	92.92	0.49	4.1	1.55	1.06	0.15	1.33	7
12X-2, 33-34	101.73	0.76	6.3	1.85	1.09	0.15	0.46	7
12X-6, 33-34	107.53	0.86	7.2	ND	ND	ND	ND	ND
13X-2, 33-34	111.33	0.53	4.4	1.76	1.23	0.16	0.99	8
13X-6, 33-34	115.85	0.49	4.1	ND	ND	ND	ND	ND
14X-2, 33-34	121.03	0.62	5.2	ND	ND	ND	ND	ND
14X-5, 69-70	125.89	0.56	4.6	2.00	1.44	0.18	0.75	8
15X-1, 27-28	128.97	0.17	1.4	1.27	1.10	0.17	1.62	6
16X-2, 34-35	140.14	0.73	6.0	2.14	1.41	0.19	1.40	7
16X-4, 34-35	143.14	0.60	5.0	ND	ND	ND	ND	ND
17X-2, 32-33	149.72	0.44	3.6	ND	ND	ND	ND	ND
17X-2, 113-114	150.53	1.42	11.8	2.82	1.40	0.12	0.59	11
18X-2, 114-115	160.14	0.44	3.7	2.24	1.80	0.23	0.76	8
18X-CC, 27-28	161.49	0.16	1.3	ND	ND	ND	ND	ND
19H-3, 93-94	171.03	0.20	1.7	2.29	2.09	0.21	0.74	10
19H-6, 34-35	174.64	0.07	0.6	ND	ND	ND	ND	ND
20X-2, 129-130	179.39	0.55	4.6	1.47	0.92	0.14	1.92	7
20X-4, 33-34	181.43	0.37	3.1	ND	ND	ND	ND	ND
21X-4, 34-35	190.84	0.13	1.1	1.01	0.88	0.11	0.49	8
22X-2, 32-33	197.42	0.58	4.9	1.12	0.54	0.09	0.06	6
22X-4, 33-34	200.43	0.25	2.1	ND	ND	ND	ND	ND
22X-6, 33-34	203.43	0.14	1.2	ND	ND	ND	ND	ND
23X-2, 33-34	207.03	0.20	1.6	0.91	0.71	0.13	0.24	5
23X-4, 33-34	210.03	0.09	0.7	ND	ND	ND	ND	ND
23X-6, 33-34	213.03	0.09	0.7	ND	ND	ND	ND	ND
24X-3, 124-125	219.04	0.18	1.5	1.00	0.82	0.13	0.48	6
24X-6, 34-35	222.64	0.15	1.2	ND	ND	ND	ND	ND
25X-2, 34-35	226.34	0.44	3.6	ND	ND	ND	ND	ND
25X-3, 119-120	228.69	0.36	3.0	1.14	0.78	0.14	0.27	6
25X-6, 34-35	232.34	0.74	6.1	ND	ND	ND	ND	ND
26X-2, 34-35	235.94	0.09	0.7	ND	ND	ND	ND	ND
26X-4, 34-35	238.94	0.46	3.8	0.79	0.33	0.09	0.26	4

Notes: IC = inorganic carbon, $CaCO_3$ = calcium carbonate, TC = total carbon, TOC = total organic carbon, TN = total nitrogen, and TS = total sulfur. ND = not determined.

This table also appears on the volume CD-ROM.

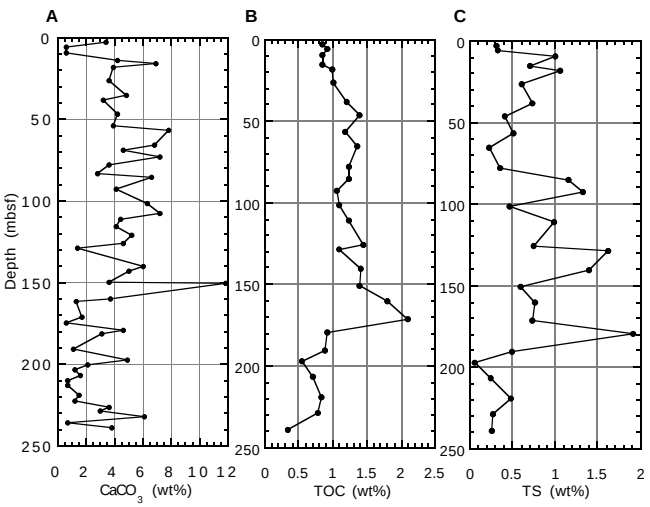

Figure 23. Concentrations of (**A**) carbonate, (**B**) total organic carbon (TOC), and (**C**) total sulfur (TS) vs. depth.

surements on core specimens are made on material extracted from the fractured cores, and therefore do not take fracture porosity into account, whereas the GRA densities measure both original fracture porosity and the additional effects of any drilling disturbance (Fig. 1). Residual discrepancies between log, discrete specimen, and GRA whole-core densities may be the result of poor hole conditions.

In the uppermost 72 m, the bulk density values gradually increase with depth from 1.6 to 1.8 g/cm^3. A large negative excursion down to 1.1 g/cm^3 from the baseline (1.8 g/cm^3) occurs in the interval 72–75 mbsf, which is correlated to the interval characterized by a geochemical anomaly (see "Geochemistry" section, this chapter). The log shows a broad negative excursion down to 1.3 g/cm^3 in the interval 88–107 mbsf. Two obvious negative excursions are identified in the intervals 123–125 mbsf and 137–139 mbsf. All negative excursions in the upper 150 mbsf are correlated with the relatively large standoff of up to 7.5 cm, as indicated by the differential caliper log (Fig. 25).

The bulk density log shows a distinct excursion down to 1.2 g/cm^3 from the baseline (1.6 g/cm^3) in an interval 146–148 mbsf (Fig. 25). This depth is close to the structurally and biostratigraphically defined décollement, which lies at 150.6 mbsf in Hole 1043B, (see "Lithostratigraphy and Structure" and "Biostratigraphy and Magnetostratigraphy" sections, this chapter). Below the décollement, in situ bulk densities range from 1.4 to 1.7 g/cm^3 in Hole 1043B, similar to

Table 14. Gamma-ray attenuation (GRA) bulk density data for Site 1043.

Leg	Site	Hole	Core	Type	Section	Top (cm)	Bottom (cm)	Depth (mbsf)	GRA density (g/cm^3)	Measured counts	Actual daq period (s)	Core diameter (cm)
170	1043	A	1	H	1	4.7	4.7	0.05	1.363	107502	5	6.7
170	1043	A	1	H	1	6.7	6.7	0.07	1.376	106774	5	6.7
170	1043	A	1	H	1	8.7	8.7	0.09	1.376	106756	5	6.7
170	1043	A	1	H	1	10.7	10.7	0.11	1.332	109398	5	6.7
170	1043	A	1	H	1	12.7	12.7	0.13	1.346	108567	5	6.7
170	1043	A	1	H	1	14.7	14.7	0.15	1.404	105094	5	6.7
170	1043	A	1	H	1	16.7	16.7	0.17	1.31	110769	5	6.7
170	1043	A	1	H	1	18.7	18.7	0.19	1.313	110560	5	6.7
170	1043	A	1	H	1	20.7	20.7	0.21	1.353	108153	5	6.7
170	1043	A	1	H	1	22.7	22.7	0.23	1.384	106300	5	6.7

Note: Daq = data acquisition

This is a sample of the table that appears on the volume CD-ROM.

Table 15. Moisture and density data, and calculated phase relationships from discrete core specimens, Site 1043.

Leg	Site	Hole	Core	Type	Section	Top (cm)	Bottom (cm)	Depth (mbsf)	Beaker number	Beaker mass (g)	Beaker volume (g/cm^3)	Wet volume (g/cm^3)	Dry volume (g/cm^3)	Wet mass (g)	Dry mass (g)
170	1043	A	1	H	1	70	72	0.7	33	8.11	3.65		6.73	23.16	15.93
170	1043	A	1	H	1	18	20	0.18	37	8.19	3.69		6.18	22.86	14.48
170	1043	A	1	H	1	125	127	1.25	39	8.18	3.68		6.13	17.63	14.56
170	1043	A	1	H	2	62	64	2.12	34	8.18	3.69		6.92	23.16	16.63
170	1043	A	1	H	2	63	65	2.13	41	8.27	3.72		8.38	26.5	19.41
170	1043	A	1	H	2	18	20	1.68	43	8.22	3.7		6.23	21.65	14.52
170	1043	A	1	H	3	27	29	3.27	45	7.94	3.58		6.63	22.11	15.64
170	1043	A	1	H	3	83	85	3.83	47	7.99	3.6		6.66	21.18	15.66
170	1043	A	1	H	3	124	126	4.24	49	8.06	3.63		6.94	21.52	16.57
170	1043	A	1	H	4	126	128	5.76	36	8.15	3.67		6.52	21.17	15.26

Table 15 (continued).

Leg	Site	Hole	Core	Type	Section	Top (cm)	Bottom (cm)	Depth (mbsf)	Water content (wet)	Water content (dry)	Wet bulk density (g/cm^3)	Dry bulk density (g/cm^3)	Grain density (g/cm^3)	Porosity (%)	Void ratio
170	1043	A	1	H	1	70	72	0.7	0.5	0.99	1.46	0.74	2.56	71.22	2.47
170	1043	A	1	H	1	18	20	0.18	0.59	1.45	1.35	0.55	2.55	78.3	3.61
170	1043	A	1	H	1	125	127	1.25	0.34	0.51	1.72	1.14	2.62	56.47	1.3
170	1043	A	1	H	2	62	64	2.12	0.45	0.82	1.54	0.84	2.63	67.9	2.12
170	1043	A	1	H	2	63	65	2.13	0.4	0.68	1.56	0.93	2.4	61.27	1.58
170	1043	A	1	H	2	18	20	1.68	0.55	1.22	1.4	0.63	2.51	74.96	2.99
170	1043	A	1	H	3	27	29	3.27	0.47	0.9	1.49	0.79	2.53	69	2.23
170	1043	A	1	H	3	83	85	3.83	0.43	0.77	1.54	0.87	2.52	65.31	1.88
170	1043	A	1	H	3	124	126	4.24	0.38	0.62	1.63	1.01	2.58	60.83	1.55
170	1043	A	1	H	4	126	128	5.76	0.47	0.89	1.49	0.79	2.51	68.48	2.17

This is a sample of the table that appears on the volume CD-ROM.

the density variation in Hole 1039D (see "Physical Properties" section, "Site 1039" chapter, this volume). A distinct increase in density occurs at 285 mbsf, which coincides with the top of nannofossil ooze in Hole 1039B (see "Site 1039" chapter, this volume). Large excursions in the intervals 310–315 mbsf and 370–390 mbsf correlate with the diatom-rich zones in Hole 1039B (see "Site 1039" chapter, this volume).

Porosities calculated directly from the neutron log fluctuate widely throughout the logged interval. Porosity values greater than 100% were removed, and the data set was smoothed by calculating a 9-pt. running average. The filtered profile (Fig. 24) ranges from 50% to 80% in porosity and is roughly compatible with the density log throughout the hole. The negative excursions in density in the intervals 72–75, 88–107, 123–125 mbsf, and the décollement (146–148 mbsf) coincide with positive excursions in neutron porosity.

Natural Gamma Ray

Laboratory Measurements on Cores

Natural gamma-ray measurements (Fig. 26A; Table 17) show remarkably little variation in the upper 230 m of Hole 1043A, with an average total count of 35–40 counts per second (cps). Two localized increases in total count up to 50 cps occur at depths of 170 and 235 mbsf, although these depths do not correspond to any obvious feature in the lithostratigraphy. The total gamma-ray count decreases uniformly to 20–25 cps over the depth range 240–282 mbsf. The decrease in natural radioactivity probably represents the decrease in clay mineral content over this interval, which extends from the base of Subunit U2A (245 mbsf) through the clayey beds of Subunit U2B (245–264 mbsf) and the nannofossil ooze and calcareous clay of Subunit U3A (263–282 mbsf).

Downhole Measurements

In situ natural gamma-ray measurements were collected by CDR in Hole 1043B (Figs. 24, 25; Table 16). The log responds to mineralogic composition and therefore indicates changes in lithology.

In the uppermost 72 m, the gamma-ray values range from 40 to 60 cps. A large negative excursion down to 15 cps from the baseline (50 cps) occurs in the interval 72–75 mbsf, which is correlated to the interval's porosity increase and coincident geochemical anomaly (see "Geochemistry" section, this chapter). The log fluctuates between 10

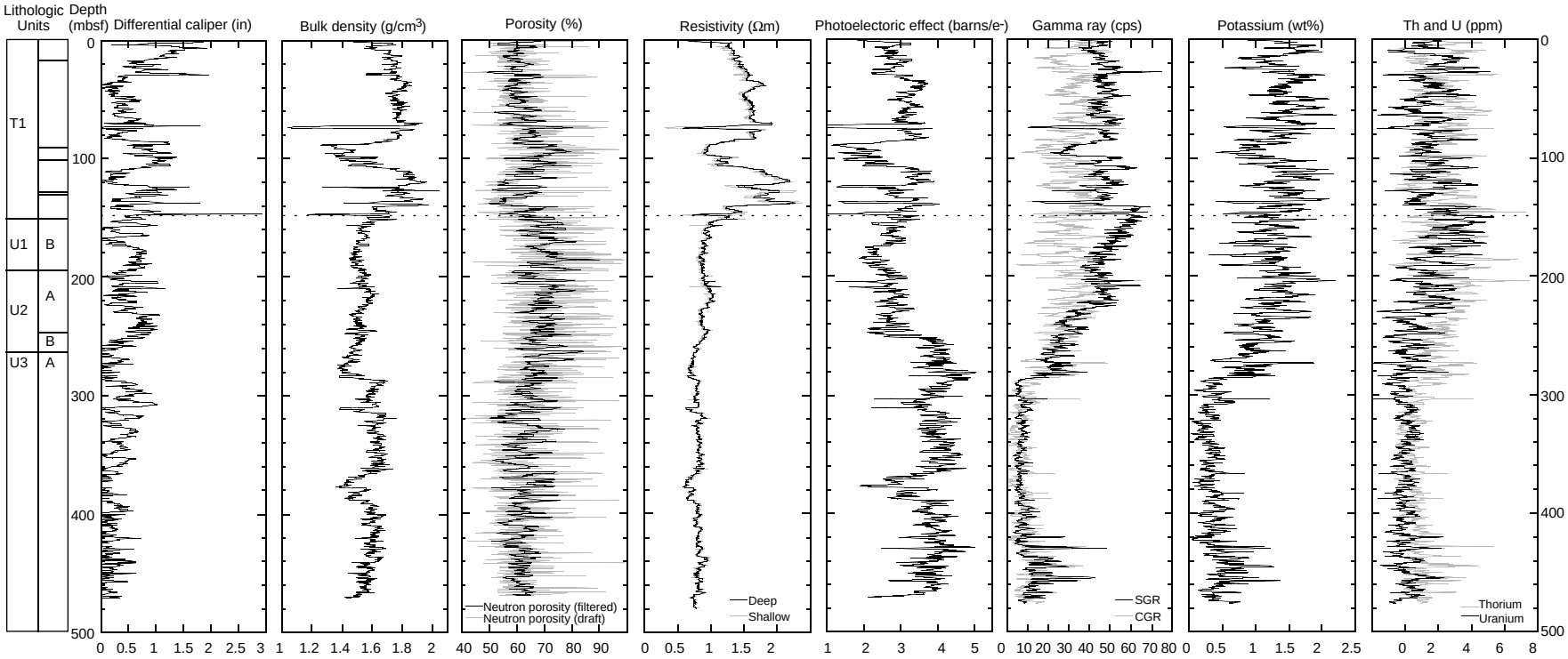

Figure 24. Summary of LWD results at Hole 1043B with lithologic units at Hole 1043A. SGR = total spectral gamma ray, CGR = computed spectral gamma ray.

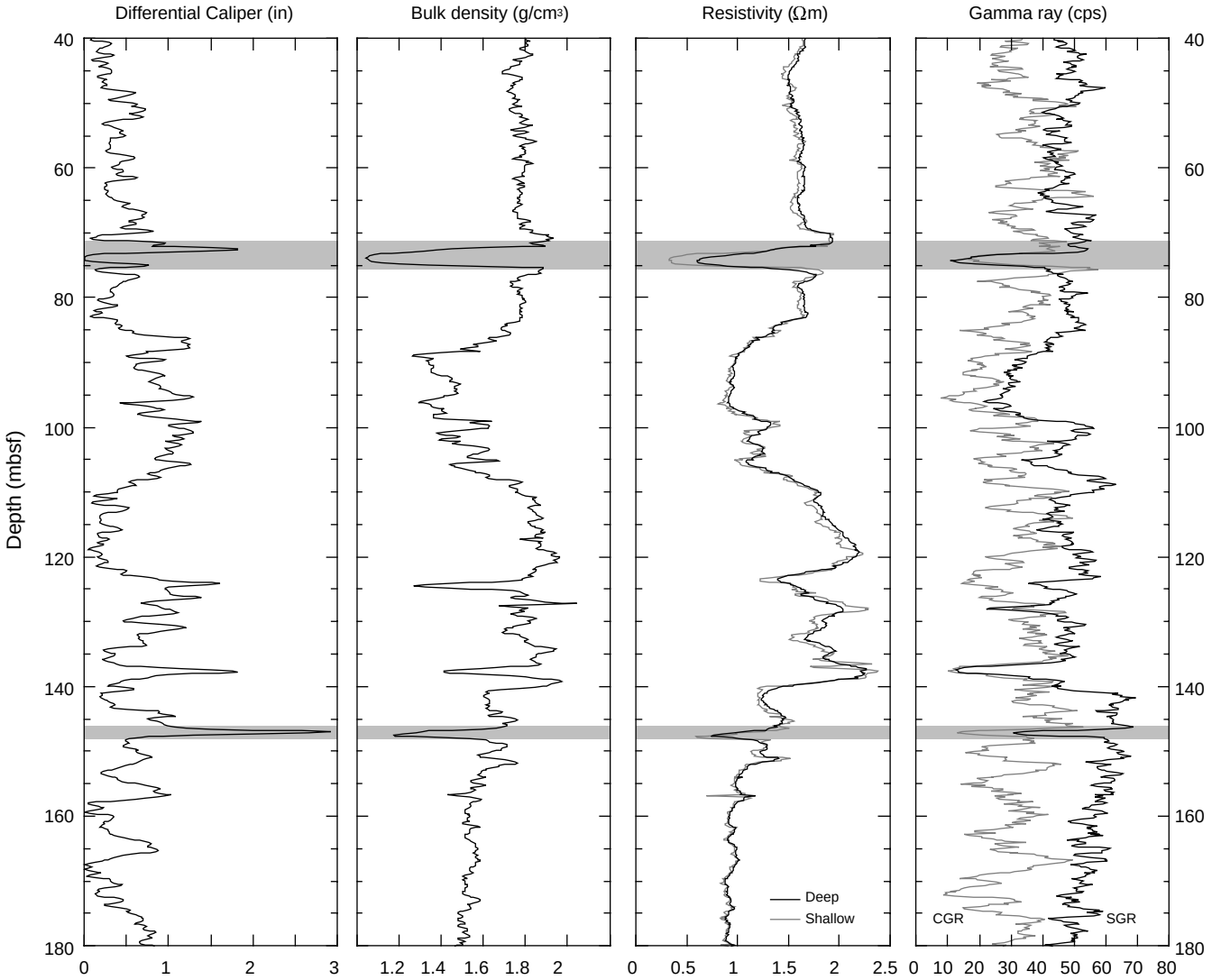

Figure 25. Differential caliper, bulk-density, resistivity, and spectral gamma-ray logs through the décollement and inferred major fault (shaded zones) at Site 1043. SGR = total spectral gamma ray, CGR = computed spectral gamma ray.

Table 16. Shipboard composite logging-while-drilling data from Hole 1043B.

Depth (mbrf)	Depth (mbsf)	ROP5 (m/hr)	ATR (Ωm)	PSR (Ωm)	RTIM (s)	GTIM (s)	GRA (GAPI)	THOR (ppm)	URAN (ppm)	POTA (wt%)	CGR (cps)	SGR (cps)	DTAB (s)	PEF (barns/e⁻)	DRHO (g/cm³)	DC_A (in)	ROMT (g/cm³)	NTAB (s)	TNPH (v/v)
4319	0.02	–999.25	0.41	0.44	200	420	19.28	0.49	0.11	0.61	12.64	13.67	1160	0.72	–0.04	0.95	1.19	1510	0.63
4319.2	0.17	–999.25	0.41	0.44	190	430	29.72	0.64	0.4	0.8	16.47	20.06	1170	1.21	–0.04	1.2	1.26	1520	0.64
4319.3	0.32	–999.25	0.55	0.63	200	450	37.56	1.16	0.46	0.96	21.05	25.12	1190	1.5	–0.04	1.31	1.33	1540	0.73
4319.5	0.47	–999.25	0.55	0.63	200	470	42.65	1.47	0.65	1.02	23.18	28.92	1230	1.67	–0.04	1.28	1.36	1570	0.66
4319.6	0.63	–999.25	0.6	0.6	130	410	45.27	1.01	1.45	0.88	19.26	32.16	1170	1.75	–0.04	1.27	1.37	1510	0.62
4319.8	0.78	–999.25	0.6	0.6	110	420	46.83	0.89	1.57	0.93	19.67	33.59	1180	1.82	–0.04	1.32	1.38	1520	0.6
4319.9	0.93	–999.25	0.67	0.71	120	440	50.23	1.09	1.7	0.97	21.07	36.2	1200	1.85	–0.04	1.42	1.39	1540	0.66
4320.1	1.08	–999.25	0.67	0.71	110	450	52.71	1.16	2.13	0.89	19.89	38.84	1220	1.89	–0.04	1.55	1.41	1550	0.82
4320.2	1.24	–999.25	0.73	0.69	100	440	53.36	1.15	2	0.97	21.29	39.02	1220	1.95	–0.05	1.69	1.44	1550	0.84
4320.4	1.39	–999.25	0.8	0.74	110	460	57.02	1.4	1.71	1.16	25.46	40.65	1260	2.05	–0.06	1.8	1.47	1580	0.67

Note: ROP5 = 5-ft averaged rate of penetration, ATR = attenuation resistivity, PSR = phase shift resistivity, RTIM = resistivity time after bit, GTIM = gamma ray time after bit, GRA = gamma ray, THOR = thorium, URAN = uranium, POTA = potassium, CGR = computed gamma ray (thorium + potassium), SGR = total gamma ray, DTAB = density time after bit, PEF = photoelectric factor, DRHO = bulk density correction, DC_A = differential caliper, ROMT = rotationally processed density, NTAB = neutron time after bit, and TNPH = thermal neutron porosity.

This is a sample of the table that appears on the volume CD-ROM.

and 60 cps in the interval 75–140 mbsf. The largest increase in total spectral gamma ray from 10 to 65 cps occurs at 140 mbsf.

The LWD total spectral gamma-ray log shows a distinct negative excursion down to 30 cps from the baseline (60 cps) in the interval 146–148 mbsf, which is believed to span the décollement zone. Below the décollement, the total gamma-ray values decrease with depth from 70 to 40 cps in the interval 150–195 mbsf. A decrease in total gamma-ray values occurs at 285 mbsf, which probably correlates with the top of nannofossil ooze in Hole 1039B (see "Site 1039" chapter, this volume). A number of excursions in gamma-ray values in the intervals 420–470 mbsf may then be correlated with the ash layers within Subunit U3B in Hole 1039B (see "Site 1039" chapter, this volume).

P-wave Velocities

P-wave velocities on unsplit cores could be measured with the *P*-wave logger (PWL) only in the APC-cored sections of Hole 1043A, which included the depth intervals 0–16 mbsf and 167–177 mbsf (Fig. 26B; Table 18). Velocities using the PWS3 transducers on split cores (Table 19) were measured elsewhere, but were unsuccessful over the depth interval 25–140 mbsf, probably due to microfractures or drilling disturbance from the XCB corer.

Within the uppermost breccia and clay layer of Unit T1, velocities increase rapidly with depth from 1530 m/s at the seafloor to 1680 ±50 m/s at 10 mbsf. Velocities increase slightly to 1700 m/s at 20 mbsf. Below this depth, a velocity near 1750 m/s was measured at 140 mbsf just above the décollement. Velocities could be tracked across the décollement at 150 mbsf, decreasing rapidly from 1720 m/s at 148 mbsf to 1585 m/s at 153 mbsf. However, a few higher velocities of 1650–1700 m/s were measured 20 m below the décollement in Core 170-1043A-19H (170 mbsf). Velocities are low throughout the diatomaceous ooze and clay of lithologic Unit U1 and the silty clay of Unit U2, with values in the range of 1550–1580 m/s down to 265 mbsf. Similar velocities are found for the calcareous clay and ooze of Subunit U3A, although it is expected that laboratory-measured velocities for the calcareous material may not represent the in situ values because of the effects of decompaction.

Synthetic Seismogram

A synthetic seismogram was created from the velocity and density data sets collected at Site 1043 to tie core-derived structure and stratigraphy data to the seismic-reflection data of Line CR-20 (Fig. 2, "Site 1040" chapter, this volume). Velocity data were assembled from core measurements obtained with the PWS3 (0–16 mbsf and 144–282 mbsf). To complete part of the profile, velocities were linearly interpolated across the data gap between 16 and 144 m. The remainder of the hole, from 282 to 482 m, was not cored because of lack of time and because previous drilling at Sites 1039 and 1040, which flank Site 1043, had sampled this section. As a means of completing the velocity profile to the total depth, laboratory-measured velocities at the adjacent sites were interpolated to the Site 1043 position. Site 1039 velocities were assumed applicable to the base of the landward trench slope. Because the principal stratigraphic boundaries were identifiable in the LWD logs, the velocity interpolation

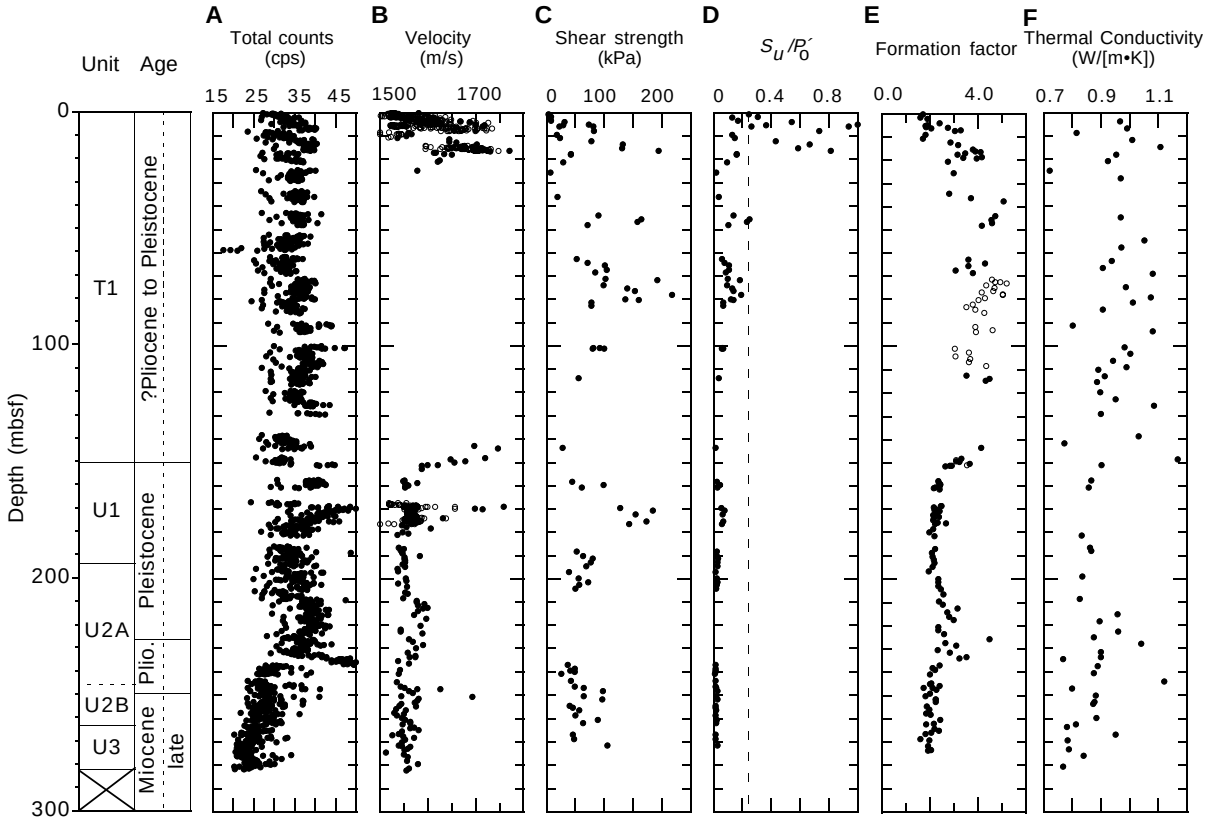

Figure 26. **A.** Natural gamma-ray radiation measured with the MST on cores from Site 1043. **B.** Acoustic compressional-wave (*P*-wave) velocity, measured directly on unsplit cores by the PWL on the MST (open circles) and on split cores by the PWS3 transducer (solid circles). **C.** Undrained shear strength, measured with the automated vane shear device, vs. depth at Site 1043. **D.** Shear strength to effective overburden stress ratio (S_u/P_0') plotted as a function of depth. Typically normally consolidated sediment has a ratio of about 0.25 (dashed line). Intervals where values exceed 0.25 indicate overconsolidation. **E.** Formation factor (the ratio of sediment resistivity to pore-fluid resistivity), derived from split cores, plotted with depth for Site 1043 (solid circles = longitudinal, open circles = transverse). **F.** Thermal conductivity vs. depth for Site 1043.

was done at specific levels in the stratigraphic section, thus taking into account the changes in stratigraphic thickness. The main feature of the available velocity data is the well-defined décollement at 150 mbsf, where measured velocity drops from ~1730 to 1587 m/s in only a few meters. Density data used for the synthetic seismogram were compiled from LWD bulk density (Hole 1043B) in the intervals 0–81 mbsf and 110–472 mbsf. LWD measurements were not used in the intervening section, 81–110 mbsf, where they were deemed unreliable. In this zone, the density measurements were anomalously low relative to the laboratory-measured densities. They coincided with an enlarged part of the hole, as indicated by the caliper, and they produced a high-amplitude, unmatched arrival in preliminary synthetic seismic data. The only other adjustment to the LWD profile was the addition of several points to the bottom of the hole (472–484 mbsf) to extrapolate 12 m of section to basement contact (gabbro). The composite velocity and density profiles, sampled at 2-m depth intervals, were combined to form an acoustic impedance series, and a reflectivity series was computed at a 1-ms sample interval. A wavelet derived from the seafloor reflection was convolved with the reflectivity series to produce the synthetic traces shown in Figure 27.

The synthetic data produced in this process coherently match the observed seismic data at Site 1043. This outcome allows a detailed correlation of the stratigraphic and structural data from recovered cores to reflection arrivals on Line CR-20. These correlations are consistent with synthetic ties at both Sites 1039 and 1040. Similar to Site 1040, the zone above the décollement at Site 1043 (from 5730 to 5910 ms two-way traveltime) on seismic Line CR-20 shows few reflections. The upper plate events in the synthetic data do not clearly match observable events on Line CR-20; however, at least one event in the synthetic data, at ~5810 ms, is associated with a subtle reflection event and a zone of anomalous pore-fluid chemistry. The décollement is marked by a large negative deflection in the synthetic trace, but does not fully match the observed seismic waveform over this interval, apparently because of the complexity in the density pro-

Table 17. Natural gamma-ray data obtained on unsplit core with the MST, Site 1043.

Leg	Site	Hole	Core	Type	Section	Top (cm)	Bottom (cm)	Depth (mbsf)	Total counts (cps)	Actual daq period (s)	Core diameter (cm)
170	1043	A	1	H	1	10.4	10.4	0.1	27.2	30	6.7
170	1043	A	1	H	1	20.4	20.4	0.2	31.67	30	6.7
170	1043	A	1	H	1	30.4	30.4	0.3	29.8	30	6.7
170	1043	A	1	H	1	40.4	40.4	0.4	29.43	30	6.7
170	1043	A	1	H	1	50.4	50.4	0.5	30.17	30	6.7
170	1043	A	1	H	1	60.4	60.4	0.6	29.27	30	6.7
170	1043	A	1	H	1	70.4	70.4	0.7	28.27	30	6.7
170	1043	A	1	H	1	80.4	80.4	0.8	32.13	30	6.7
170	1043	A	1	H	1	90.4	90.4	0.9	31.33	30	6.7
170	1043	A	1	H	1	100.4	100.4	1	29.8	30	6.7

Note: Daq = data acquisition.

This is a sample of the table that appears on the volume CD-ROM.

Table 18. *P*-wave velocities obtained from the PWL using the MST on unsplit cores from Site 1043.

Leg	Site	Hole	Core	Type	Section	Top (cm)	Bottom (cm)	Depth (mbsf)	Velocity (m/s)	Meas. separation mean (mV)	Meas. separation SD (mV)	Meas. time mean (µs)	Meas. time SD (µs)	Acoustic level mean	Attempted daq	Valid daq	Liner thickness (mm)
170	1043	A	1	H	1	6.3	6.3	0.06	1529.9	205	0	50.95	0.04	169	25	5	2.54
170	1043	A	1	H	1	8.3	8.3	0.08	1527.5	205	0	51.02	0.024	187	25	25	2.54
170	1043	A	1	H	1	10.3	10.3	0.1	1521.8	204	0	51.12	0.024	202	25	25	2.54
170	1043	A	1	H	1	12.3	12.3	0.12	1528.7	204	0	50.92	0.025	197	25	25	2.54
170	1043	A	1	H	1	14.3	14.3	0.14	1532.6	204	0	50.81	0.018	191	0	25	2.54
170	1043	A	1	H	1	16.3	16.3	0.16	1517	204	0	51.26	0.018	218	25	25	2.54
170	1043	A	1	H	1	18.3	18.3	0.18	1516.7	204	0	51.27	0.025	223	25	2	2.54
170	1043	A	1	H	1	20.3	20.3	0.2	1523.5	204	0	51.07	0.025	219	25	25	2.54
170	1043	A	1	H	1	22.3	22.3	0.22	1529.1	204	0	50.91	0.016	223	25	2	2.54
170	1043	A	1	H	1	24.3	24.3	0.24	1524.9	204	0	51.03	0.025	225	25	25	2.54

Note: SD = standard deviation, daq = data acquisition.

This is a sample of the table that appears on the volume CD-ROM.

Table 19. *P*-wave velocities obtained from the PWS3 on split cores from Site 1043.

Leg	Site	Hole	Core	Type	Section	Top (cm)	Bottom (cm)	Depth (mbsf)	Velocity (m/s)	Distance (mm)	Time (µs)	Liner thickness (mm)
170	1043	A	1	H	1	10.5	10.5	0.11	1581.7	36.07	23.42	2.64
170	1043	A	1	H	2	18.3	18.3	1.68	1557.9	35.1	23.12	2.64
170	1043	A	1	H	2	55.7	55.7	2.06	1551.3	40.61	26.76	2.64
170	1043	A	1	H	2	56	56	2.06	1552.1	38.81	25.96	0
170	1043	A	1	H	2	82	82	2.32	1610.8	38.2	24.36	2.64
170	1043	A	1	H	2	116.3	116.3	2.66	1609.4	39.17	24.982	2.64
170	1043	A	1	H	3	55.3	55.3	3.55	1667.5	38.63	23.868	2.64
170	1043	A	1	H	3	82.3	82.3	3.82	1688	36.22	22.177	2.64
170	1043	A	1	H	4	41.1	41.1	4.91	1699.8	36.46	22.18	2.64
170	1043	A	1	H	4	45.4	45.4	4.95	1629.6	39.08	24.646	2.64

This is a sample of the table that appears on the volume CD-ROM.

file. Below the décollement, the designated unit boundaries of the underthrust section are easily identified. The exceptions to this are Subunit U1A and the top of Subunit U1B, which are missing. As expected, because of the lack of full velocity control, the times of events in the synthetic data do not accurately match the correlative observed events.

Magnetic Susceptibility

Magnetic susceptibility (Fig. 1; Table 20) is high in the upper 10 mbsf, corresponding to the uppermost layer of breccia and clay within Unit T1. From 10 to 75 mbsf, a number of large positive excursions in susceptibility values are observed. This pattern contrasts with the more uniform and lower values of magnetic susceptibility in the interval from 75 to 126 mbsf. In the lowermost part of Unit T1, two additional excursions are noted at depths of 130 and 145 mbsf.

Within the underthrust sedimentary section, the magnetic susceptibility measurements provide many identifying features that can be correlated both to the reference section at Site 1039 and to the underthrust section farther landward at Site 1040. As at Site 1040, a positive excursion (at a depth of 152 mbsf) is observed just below the décollement. The largest peak in susceptibility values for Site 1043 occurs at 175 mbsf, which can be correlated confidently with the peak at 45 mbsf for Site 1039 (Fig. 1, "Site 1039" chapter, this volume). This peak, and others within Subunit U1B, are associated with widely distributed ash layers. Similarly, the clearly defined pattern in susceptibility values from 205 to 242 mbsf for Site 1043 is also easily identified at Sites 1039 and 1040. Another clear marker is the susceptibility peak in Subunit U3A at a depth of 275 mbsf. Because the corresponding peak for Site 1039 was found 20 m above the base of Subunit U3A, the susceptibility data indicate that the top of the nannofossil ooze Subunit U3B should be located less than 10 m below a depth of 282 mbsf, which was the maximum depth cored at Hole 1043A.

Vane Shear Strength

Excellent core recovery and lower sediment induration allowed shear strength measurements to be taken over a large depth interval (Fig. 26A; Table 21). Shear strength increases rapidly with depth over the first 14 m, reaching a peak value of 196 kPa. This increase suggests progressive consolidation within the uppermost breccia and clay layer. Below this depth, shear strength values become more varied, probably associated with XCB-coring disturbances. However, several minor trends of increasing strength appear to occur within specific intervals. Between 60 and 80 mbsf, an almost linear increase occurs from 55 to 160 kPa. No lithologic variation explains this increase, and therefore strength variations could represent consolidation fluctuation within certain intervals of Unit T1. A similar trend is observed below the décollement (150 mbsf); shear strength increases from 40 to 170 kPa over a 22-m-thick interval. Normalizing the shear strength data with respect to calculated overburden pressure (obtained using wet bulk density measurements and assuming hydrostatic conditions) shows that the upper 16 m of sediment is generally overconsolidated (Fig. 26D). Below this depth, the sediment becomes increasingly more underconsolidated. This is consistent with the high porosity values that increase with depth throughout the whole section.

Electrical Resistivity

Laboratory Measurements

Good core quality and the relatively soft nature of the sediment made it possible to collect electrical resistivity data on split cores along almost the entire recovered interval. One or two measurements were taken per section (Fig. 26E; Table 22). Between 115 and 140 mbsf, the sediments were too firm or brittle for the probe to be properly inserted.

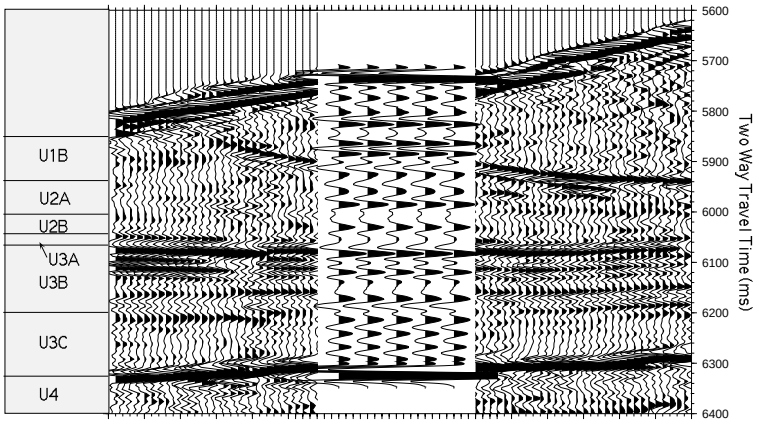

Figure 27. Line CR-20 seismic-reflection data in the vicinity of Site 1043 with synthetic seismic traces inserted at the Site 1043 location. Lithostratigraphic units of the lower plate undertrusting the margin are indicated at the left; Unit T1 occurs at the right from the surface to 5930 ms depth and represents the upper plate.

Table 20. Magnetic susceptibility values obtained on unsplit cores using the MST, Site 1043.

Leg	Site	Hole	Core	Type	Section	Top (cm)	Bottom (cm)	Depth (mbsf)	Relative, drift corr. sus.	Relative sus. mean	Actual daq period (s)	Core diameter (cm)	Sample elapsed zero time (s)	Drift correction
170	1043	A	1	H	1	4	4	0.04	186.1	186	5	6.7	8009	–0.1
170	1043	A	1	H	1	6	6	0.06	217.1	217	5	6.7	11447	–0.1
170	1043	A	1	H	1	8	8	0.08	231.9	231.8	5	6.7	14880	–0.1
170	1043	A	1	H	1	10	10	0.1	222.5	222.4	5	6.7	18314	–0.1
170	1043	A	1	H	1	12	12	0.12	204.9	204.8	5	6.7	21731	–0.1
170	1043	A	1	H	1	14	14	0.14	199.6	199.4	5	6.7	25140	–0.2
170	1043	A	1	H	1	16	16	0.16	216.6	216.4	5	6.7	28551	–0.2
170	1043	A	1	H	1	18	18	0.18	240.2	240	5	6.7	31966	–0.2
170	1043	A	1	H	1	20	20	0.2	260	259.8	5	6.7	35375	–0.2
170	1043	A	1	H	1	22	22	0.22	272.7	272.4	5	6.7	38824	–0.3

Note: Corr. = corrected, sus. = susceptibility, daq = data acquisition.

This is a sample of the table that appears on the volume CD-ROM.

Between the seafloor and 20 mbsf, the resistivity increases from low values of just over 0.3 to 0.9 Ωm. Between 20 and 36 mbsf, few measurements were made, but resistivity appears to decrease to values close to 0.6 Ωm. Between 35 and 65 mbsf and between 65 and 115 mbsf, the data show two ill-defined bands of decreasing resistivity with depth (average values decrease from around 1.0 Ωm to less than 0.7 Ωm in both cases).

Resistivity was measured in the split cores throughout the interval containing the décollement zone. Between 148 and 150 mbsf, values are around 0.64 Ωm. Immediately below the décollement boundary (150.67 mbsf), the resistivity increases to 0.74 Ωm then decreases over the next 3 m to values of around 0.5 Ωm. The measured resistivity values remain between 0.4 and 0.5 Ωm to a depth of ~205 mbsf, where they become considerably more scattered and indicate a general increase in sediment resistivity. Values measured return to values of between 0.34 and 0.52 Ωm from 236 mbsf to the bottom of the recovered interval.

Values of formation factor (Fig. 26E) were calculated throughout assuming a constant pore-water salinity of 35‰ and a constant core temperature of 23.5°C, and therefore show exactly the same trends as the resistivity data described above.

Downhole Measurements

In situ resistivity measurements were collected using the CDR in Hole 1043B (Table 16). The deep and shallow resistivity logs shown in Figures 24 and 25 show very similar trends and amplitudes, indicating good hole conditions. The resistivity log shows similar variations as the bulk density log throughout Hole 1043B.

A distinct negative excursion down to 0.6 Ωm from the baseline (1.2 Ωm) is observed in the décollement zone (146–148 mbsf; Fig. 25). A large negative excursion down to 0.5 Ωm from the baseline (~1.5 Ωm) occurs in the interval 72–76 mbsf, which is correlated to the intervals of large negative excursion of bulk density and gamma ray. Below the décollement, the resistivity log response in Hole 1043B is similar to that in Hole 1039D (see "Physical Properties" section, "Site 1039" chapter, this volume). The values range from 0.6 to 1.0 Ωm. An increase in resistivity values occurs at 285 mbsf, which coincides with the top of nannofossil ooze in Hole 1039B (see "Site 1039", this chapter, this volume). Some excursions in the intervals 310–315 mbsf and 370–390 mbsf correlate with the diatom-rich zones in Hole 1039B (see "Site 1039" chapter, this volume).

Accurate formation factors cannot be calculated for Site 1043, because the temperature profile is not known, and there are some variations in pore-water chemistry. Approximate values can be estimated assuming constant pore-water salinity and uniform geothermal gradient similar to that measured at Site 1040B. A first order comparison suggests that formation factors derived from LWD resistivity in Hole 1043B agree reasonably well with those derived from split-core probe resistivities taken at room temperature from Hole 1043 (Fig. 26E).

Table 21. Vane shear strength data for Hole 1043A.

Leg	Site	Hole	Core	Type	Section	Top (cm)	Bottom (cm)	Depth (mbsf)	Shear strength (kPa)	Residual strength (kPa)
170	1043	A	1	H	1	70.2	70.2	0.7	2.5	0.9
170	1043	A	1	H	1	70.2	70.2	0.7	2.5	0.9
170	1043	A	1	H	2	62	62	2.12	4	2.3
170	1043	A	1	H	2	18.1	18.1	1.68	7.5	4.1
170	1043	A	1	H	3	27.1	27.1	3.27	8	5.5
170	1043	A	1	H	3	27.1	27.1	3.27	8	5.5
170	1043	A	1	H	3	82.7	82.7	3.83	30.4	27.4
170	1043	A	1	H	3	82.7	82.7	3.83	30.4	27.4
170	1043	A	1	H	4	126.2	126.2	5.76	22.1	11.3
170	1043	A	1	H	4	75	75	5.25	28.2	13.5

This is a sample of the table that appears on the volume CD-ROM.

Thermal Conductivity

Thermal conductivity data were collected on unsplit cores at two or three positions along each core, using the full-space needle probe method (Table 23). Measurements made on cored intervals that were disturbed by drilling were subsequently discarded. Values range between 0.72 and 1.18 W/(m·K) over the entire section, and although a significant amount of scatter was recorded, it is possible to relate certain trends to lithological variations (Fig. 26F). Unit T1 values remain fairly constant at an average of ~0.96 W/(m·K) between 0 and 150 mbsf, reflecting the homogeneity of the sediment. Excursions from this trend could be caused by drilling, although higher values obtained at intervals 0–10 mbsf and at 97 mbsf correspond to intervals of breccia (see "Lithostratigraphy and Structure" section, this chapter). Below the décollement, average thermal conductivity values drop to ~0.85 W/(m·K). These values change little with increasing depth, although a drop in thermal conductivity occurs at 263 mbsf at the Unit U2/U3 boundary.

Colorimetry

The lightness component (L*) of sediments drilled at Site 1043 remains fairly constant (~40%) in the upper 150 m (Figs. 1, 28). Below this depth, L* values increase to greater than 60% at 275 mbsf before dropping to nearly 40% at the base of the hole. The shallow region of relatively constant luminance corresponds to Unit T1, below which L* values increase throughout the remaining units. The highest values and the final drop both occur within Subunit U3A.

The increase in lightness over Subunits U1B through U3A does not allow their differentiation based solely on this property. The red/blue (a*/–b*) ratio, however, shows a remarkable difference between

Table 22. Electrical resistivity measurement data collected from Site 1043 cores.

Leg	Site	Hole	Core	Type	Section	Top (cm)	Bottom (cm)	Depth (mbsf)	Long. reading	Transverse reading	Temp. (°C)	Long. resistivity (Ωm)	Transverse resistivity (Ωm)	Seawater resistivity (Ωm)	Formation factor, long. (Ωm)	Formation factor, transverse (Ωm)
170	1043	A	1	H	1	50	53	0.5	5.93		22.2	0.347		0.202	1.715	
170	1043	A	1	H	2	18	21	1.68	5.53		22.2	0.323		0.202	1.6	
170	1043	A	1	H	2	78	81	2.28	6.54		22.2	0.382		0.202	1.892	
170	1043	A	1	H	3	124	127	4.24	8.33		22.2	0.487		0.202	2.41	
170	1043	A	1	H	4	49	52	4.99	6.49		22.2	0.379		0.202	1.877	
170	1043	A	1	H	4	70	73	5.2	6.32		22.2	0.37		0.202	1.828	
170	1043	A	1	H	4	133	136	5.83	6.36		22.2	0.372		0.202	1.84	
170	1043	A	1	H	5	11	14	6.11	9.54		22.2	0.558		0.202	2.76	
170	1043	A	1	H	5	47	50	6.47	7.11		22.2	0.416		0.202	2.057	
170	1043	A	1	H	5	122	125	7.22	11.33		22.2	0.662		0.202	3.278	

Note: Long. = longitudinal.

This is a sample of the table that appears on the volume CD-ROM.

Table 23. Thermal conductivity data for Site 1043.

Leg	Site	Hole	Core	Type	Section	Top (cm)	Bottom (cm)	Depth (mbsf)	Thermal conductivity (W/[m·K])
170	1043	A	1	H	3	50	50	3.5	0.967
170	1043	A	1	H	5	50	50	6.5	0.99
170	1043	A	2	H	3	50	50	11.5	1.008
170	1043	A	2	H	5	55	55	14.55	1.107
170	1043	A	2	H	1	50	50	8.5	0.814
170	1043	A	3	X	1	86	86	17.76	0.953
170	1043	A	3	X	3	62	62	20.52	0.924
170	1043	A	4	X	4	31	31	28.01	0.969
170	1043	A	4	X	1	43	43	24.83	0.722
170	1043	A	6	X	2	58	58	44.88	0.968

This is a sample of the table that appears on the volume CD-ROM.

these underthrust units (Fig. 1). Subunit U1A has a mean chromaticity ratio of 0.65, Unit U2 ranges from 0.88 (Subunit U2A) to 0.95 (Subunit U2B), and Unit 3A has an average ratio of 0.34. Unit T1 and Subunit U1B have very similar values for both lightness and red/blue ratio, making them almost indistinguishable from each other. A comparison of L* and (a*/–b*) values for each unit is given in Figure 28A.

Mean reflectance vs. wavelength curves are very similar for all units drilled at Site 1043, not only in their values but also in their shape (Fig. 28B). They all show a minimum in reflectance at 430 nm in wavelength, and they all reach their maximum values between 530 and 580 nm. Unit T1 has reflectance values of ~11% and is therefore the least reflective at all wavelengths. Unit U3A shows the highest values, ranging from 16% to 19%.

Ms 170IR-107

NOTE: Core-description forms ("barrel sheets") and core photographs can be found in Section 3, beginning on page 251. Smear-slide data and shore-based processed log data and descriptions can be found on CD-ROM. See Table of Contents for material contained on CD-ROM.

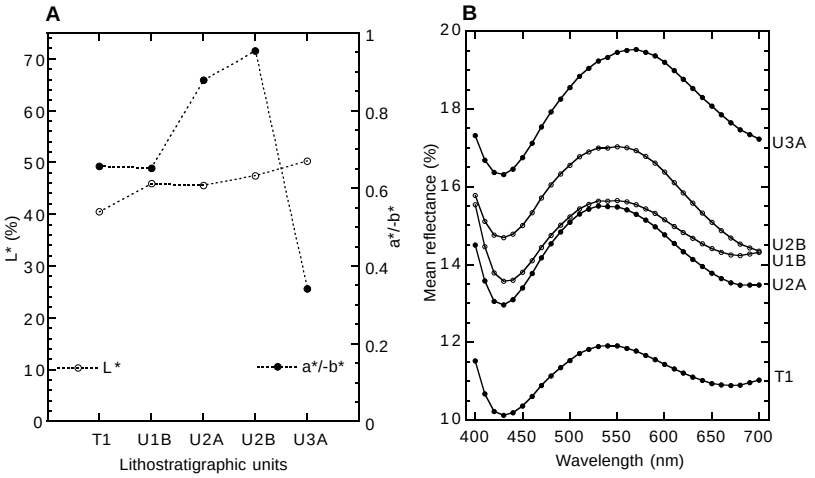

Figure 28. **A.** Mean lightness component (L*; open circles) and chromaticity ratio (a*/–b*; solid circles) for each lithostratigraphic unit drilled at Site 1043. **B.** Mean percentage of reflectance vs. wavelength for each unit cored at Site 1043.

Previous Chapter Table of Contents Next Chapter